Cellular/Molecular

In Vivo Imaging of Intersynaptic Vesicle Exchange Using VGLUT1^{Venus} Knock-In Mice

Etienne Herzog,[1,2,3,4]* Fabien Nadrigny,[5,6,7]* Katlin Silm,[2,3,4]* Christoph Biesemann,[1] Imke Helling,[9] Tiphaine Bersot,[2,3,4] Heinz Steffens,[5,11,12] Richard Schwartzmann,[8] U. Valentin Nägerl,[6,7,9] Salah El Mestikawy,[2,3,4] JeongSeop Rhee,[1] Frank Kirchhoff,[5,10] and Nils Brose[1]

[1]Department of Molecular Neurobiology, Max Planck Institute of Experimental Medicine, D-37075 Göttingen, Germany, [2]Institut National de la Santé et de la Recherche Médicale, U952, 75005 Paris, France, [3]Centre National de la Recherche Scientifique (CNRS) UMR 7224, 75005 Paris, France, [4]Université Pierre et Marie Curie (UPMC), Pathophysiology of Central Nervous System Disorders, 75005 Paris, France, [5]Department of Neurogenetics, Max Planck Institute of Experimental Medicine, D-37075 Göttingen, Germany, [6]Université de Bordeaux, 33076 Bordeaux, France, [7]CNRS, Interdisciplinary Institute for Neuroscience, UMR 5297, 33076 Bordeaux, France, [8]UPMC, Service d'Imagerie Cellulaire et Cytométrie en Flux, IFR83, 75005 Paris, France, [9]Department of Cellular and Systems Neurobiology, Max Planck Institute of Neurobiology, 82152 Martinsried, Germany, [10]Department of Physiology, University of Saarland, D-66421 Homburg, Germany, [11]Institute of Physiology, Georg August University of Göttingen, 37073 Göttingen, Germany, and [12]Department of NanoBiophotonics, Max Planck Institute of Biophysical Chemistry, 37077 Göttingen, Germany

The vesicular glutamate transporter VGLUT1 loads synaptic vesicles with the neurotransmitter glutamate and thereby determines glutamate release at many synapses in the mammalian brain. Due to its function and selective localization, VGLUT1 is one of the most specific markers for glutamatergic synaptic vesicles. It has been used widely to identify glutamatergic synapses, and its expression levels are tightly correlated with changes in quantal size, modulations of synaptic plasticity, and corresponding behaviors. We generated a fluorescent VGLUT1^{Venus} knock-in mouse for the analysis of VGLUT1 and glutamatergic synaptic vesicle trafficking. The mutation does not affect glutamatergic synapse function, and thus the new mouse model represents a universal tool for the analysis of glutamatergic transmitter systems in the forebrain. Previous studies demonstrated synaptic vesicle exchange between terminals *in vitro*. Using the VGLUT1^{Venus} knock-in, we show that synaptic vesicles are dynamically shared among boutons in the cortex of mice *in vivo*. We provide a detailed analysis of synaptic vesicle sharing *in vitro*, and show that network homeostasis leads to dynamic scaling of synaptic VGLUT1 levels.

Introduction

The first appearance of synaptic vesicles (SVs) at developing synapses marks the genesis of a transmitter release site, and subsequent SV accumulation is a key determinant of synapse maturation (Jin and Garner, 2008). Presynaptic SVs are segregated into functional pools, distinguished by their subsynaptic localization, fusion competence, and release characteristics (Galli and Haucke, 2001; Rizzoli and Betz, 2005; Wojcik and Brose, 2007). SV transport to synapses, their transfer between pools, their Ca^{2+}-triggered fusion, and their recovery by endocytosis determine the establishment, efficacy, and functional plasticity of transmitter release (Wojcik and Brose, 2007). The underlying trafficking steps have been studied almost exclusively in culture, using imaging of styryl-dye-labeled SV membranes or heterologously expressed fluorescently tagged SV proteins (Rizzoli et al., 2003; Khvotchev and Kavalali, 2008).

The present study aimed at the generation of a genetic mouse model for the fluorescence imaging of SV trafficking *in vivo*, in live neurons within intact neuronal networks. We opted for a Venus tag, a rapidly maturing and brightly fluorescing variant of the green fluorescent protein (GFP) (Nagai et al., 2002), whose variants have been used widely to image neuronal cells in many organisms (Giepmans et al., 2006). As the SV protein to be tagged, we chose the main SV glutamate transporter of glutamatergic forebrain neurons, VGLUT1 (Takamori et al., 2000), because it is an extremely accurate marker of SVs with hardly any ectopic localization (Fremeau et al., 2004a; Balaji and Ryan, 2007), it labels the most abundant glutamatergic synapses in forebrain regions that are amenable to *in vivo* two-photon imaging (Fremeau et al., 2001; Herzog et al., 2001; Sakata-Haga et al., 2001; Varoqui et al., 2002), its expression levels at synapses report SV numbers with high fidelity and correlate tightly

Received April 20, 2011; revised Aug. 24, 2011; accepted Sept. 8, 2011.

Author contributions: E.H., F.N., U.V.N., S.E.M., JS.R., and N.B. designed research; E.H., F.N., K.S., C.B., I.H., T.B., H.S., R.S., U.V.N., and JS.R. performed research; F.K. and N.B. contributed unpublished reagents/analytic tools; E.H., F.N., K.S., C.B., I.H., T.B., U.V.N., S.E.M., JS.R., and N.B. analyzed data; E.H. and N.B. wrote the paper.

This work was supported by the Max Planck Society (N.B.), the Fondation pour la Recherche Médicale (F.N.), the Agence Nationale de la Recherche (S.E.M.), the French Ministère de l'Enseignement Superieur et de la Recherche (K.S., T.B.), and the European Commission (EUROSPIN and SynSys, N.B.). We are grateful to Martin Oheim, Thierry Gally, and Sonja Wojcik for insightful discussions, to Sally Wenger and Anja Galinski for excellent technical assistance, to Stéphane Tronche and Tanja Leinert for the management of mouse colonies, and to Virginie Georget and Susanne Bolte for excellent imaging support.

*E.H., F.N., and K.S. contributed equally to this work.

Correspondence should be addressed to either of the following: Etienne Herzog, UMRS INSERM 952/CNRS 7224/UPMC, Physiopathologie des Maladies du Système Nerveux Central, Université Pierre et Marie Curie, 9 quai Saint Bernard, 75252 Paris cedex 05, France, E-mail: etienne.herzog@snv.jussieu.fr; or Nils Brose, Max Planck Institute of Experimental Medicine, Department of Molecular Neurobiology, Hermann-Rein-Str. 3, 37075 Göttingen, Germany, E-mail: brose@em.mpg.de.

DOI:10.1523/JNEUROSCI.2073-11.2011

Copyright © 2011 the authors 0270-6474/11/3115544-16$15.00/0

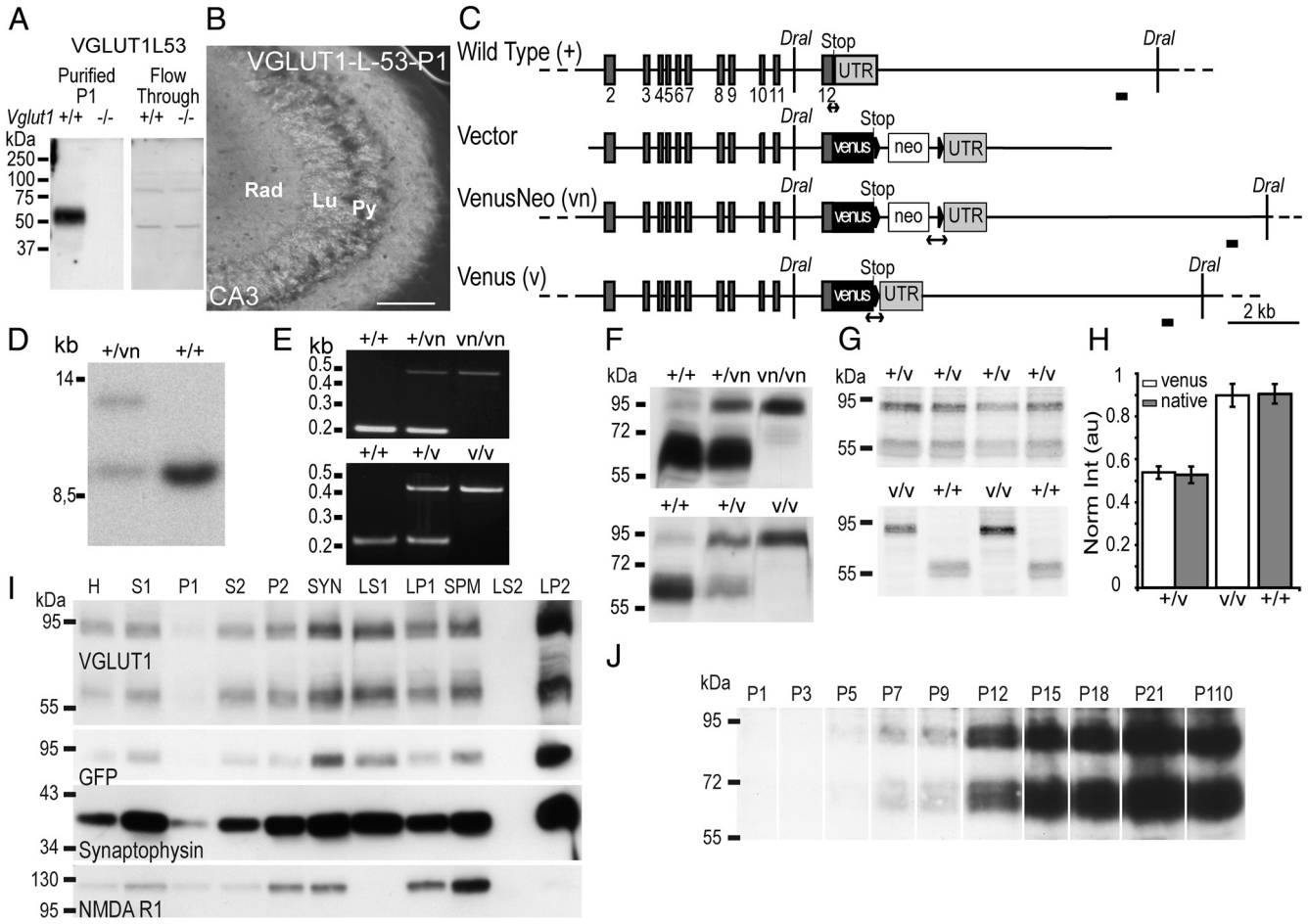

Figure 1. Generation of VGLUT1 antibodies and VGLUT1^{Venus} KIs. ***A***, Western blot comparing WT (VGLUT1 +/+) and VGLUT1 KO (VGLUT1 −/−) brain homogenates using purified VGLUT1L–53P1 antibody (left) and, as a negative control, the flow through of the antiserum after affinity purification, i.e., after the specific anti-VGLUT1 antibody fraction had been depleted. A single specific band of the size predicted for VGLUT1 is seen in WT but not in KO samples. ***B***, Immunofluorescence staining using the purified VGLUT1L–53P1 on WT hippocampus. Note the typical VGLUT1 staining of mossy fiber terminals and thinner neuropil of the stratum radiatum. CA3, Cornu ammonis area 3; Rad, stratum radiatum; Lu, stratum lucidum; Pyr, stratum pyramidale. Scale bar, 100 μm. ***C***, Strategy for the generation of the VGLUT1^{Venus} KI mutation in mouse embryonic stem cells. The WT VGLUT1 gene, the targeting vector, the mutated gene after homologous recombination (VenusNeo, vn), and the mutated gene after Cre recombination (Venus, v) are shown. Exons are indicated by gray boxes. The black triangles indicate loxP sites. A black horizontal bar indicates the probe used for Southern analysis. Double arrows represent the amplicons of PCR genotyping in the various genotypes. NEO, Neomycin resistance gene; Venus, open reading frame of Venus fluorescent protein; UTR, 3′ untranslated region. ***D***, Southern blot analysis of ES cell DNA after DraI digestion using the probe indicated in ***C***. vn, Mutated allele with neomycin resistance cassette (13.4 kbp); +, WT allele (10.2 kbp). ***E***, PCR genotyping of WT, VenusNeo, and Venus mouse tail DNA. ***F***, Comparison of VGLUT1 and VGLUT1^{Venus} expression in VenusNeo (vn) and Venus mouse lines (v). Venus-tagged VGLUT1 is ~25 kDa larger than the WT transporter. Note that the presence of the neomycin resistance cassette in the 3′ untranslated region of the VGLUT1 mRNA leads to a downregulation of VGLUT1^{Venus} expression. This is not the case after Cre-mediated removal of the neomycin resistance cassette. ***G***, ***H***, Semiquantitative Western blot analyses (near infrared fluorescent detection) of brain homogenates from +/v (0.54 ± 0.11 AU for VGLUT1^{venus} vs 0.53 ± 0.08 AU for VGLUT1; $n = 16$), v/v (0.90 ± 0.11 AU; $n = 4$), and +/+ (0.90 ± 0.08 AU; $n = 3$) mice. VGLUT2 was used as an internal loading control in the other detection channel of the system (not shown). For quantification, VGLUT1 signals were normalized to VGLUT2 signals. ***I***, VGLUT1 and VGLUT1^{Venus} in subcellular fractions of cerebral cortices from +/v mice. Fractions (10 μg of protein per lane) were separated by SDS-PAGE and analyzed by Western blotting with antibodies to the indicated proteins. The ratio between the levels of native and tagged transporters was constant throughout the fractionation when monitored using semiquantitative fluorescence analysis (not shown). H, Homogenate; S1, supernatant after sedimentation of nuclei; P1, nuclear pellet; S2, supernatant after sedimentation of crude synaptosomes; P2, crude synaptosomal pellet; SYN, sucrose density gradient purified synaptosomes; LS1, supernatant after LP1 sedimentation; LP1, lysed synaptosomal membranes; SPM, sucrose density gradient purified synaptic plasma membranes; LS2, cytosolic synaptosomal fraction; LP2, crude synaptic vesicle fraction. ***J***, Native and Venus-tagged VGLUT1 in homogenates of +/v brains at different developmental stages. The developmental expression profiles of VGLUT1 and VGLUT1^{Venus} are identical. The representative array of blots was reconstructed from selected lanes from several mice per stage blotted on the same membranes. P, Postnatal day.

with synaptic strength (Wojcik et al., 2004; De Gois et al., 2005; Wilson et al., 2005; Herzog et al., 2006; Moechars et al., 2006), and C-terminal tagging of VGLUT1 by Venus does not interfere with normal transporter function (Wojcik et al., 2004). To ensure a normal expression profile of Venus-tagged VGLUT1, we selected a knock-in (KI) mutagenesis strategy to cause expression of VGLUT1^{Venus} instead of wild-type (WT) VGLUT1 from the genomic locus *Slc17a7* (*VGLUT1*).

Our VGLUT1^{Venus} mouse line is an extremely reliable tool to image SV trafficking *in vitro* and *in vivo* that will be useful to assess synaptogenesis, presynaptic function, or SV trafficking under physiological and pathological conditions. Previous studies demonstrated SV exchange among axonal boutons *in vitro* (Darcy et al., 2006; Tsuriel et al., 2006; Chen et al., 2008; Staras et al., 2010). Using fluorescence recovery after photobleaching (FRAP) and time-lapse imaging, we show that SV pools *in vivo* do not merely recycle locally. Rather, our data further stress the complexity of the intersynaptic superpool of SVs *in vitro* and *in vivo*: SVs in this pool are dynamically exchanged between synapses to allow for increases in the VGLUT1 content of a subset of presynaptic boutons at the expense of others.

Materials and Methods

Animals. All animal experiments were performed in compliance with the European Communities Council Directive (86/809/EEC) regarding the care and use of animals for experimental procedures, the French Ministère de l'Agriculture et de la Forêt, Service Vétérinaire de la Santé et de la Protection Animale, and the guidelines for the welfare of experimental animals issued by the State Governments of Lower Saxony and Bavaria, Germany (comparable to NIH guidelines).

Antibodies. All immunodetections of VGLUT1 were performed with a custom-made affinity-purified rabbit polyclonal antibody (VGLUT1L-53P1) that had been raised against a peptide representing residues 277–290 of mouse VGLUT1 (AIGESAKLMNPVTK; Biogenes). The specificity of the antibody was assessed by immunoblotting and immunofluorescence experiments comparing WT VGLUT1 and VGLUT1 knock-out (KO) samples (Wojcik et al., 2004). In addition, control experiments were performed with antibody solutions that had been preincubated with the antigen before use (see Fig. 1*A*,*B*). The following additional primary antibodies were used: anti-Synapsin-1/2, rabbit polyclonal antiserum 106002 (Synaptic Systems); anti-GluR2 extracellular epitope, mouse monoclonal antibody 6C4 MAB397 (Millipore); anti-PSD95, mouse monoclonal antibody 6G6–1C9 ab2723 (Abcam); anti-VGLUT2, polyclonal guinea pig antiserum AB5907 (Millipore); anti-VGLUT3, rabbit polyclonal antiserum 135203 (Synaptic Systems); anti-VIAAT, polyclonal guinea pig antiserum AB2257 (Millipore); anti-GFP, monoclonal antibody 11814460001 (Roche); anti-NMDAR1, monoclonal antibody clone 54.1 (Brose et al., 1994); anti-Synaptophysin, monoclonal antibody 7.2 101011 (Synaptic Systems); and anti-c-Fos, polyclonal rabbit antiserum Sc-52 (Santa Cruz Biotechnology). The following secondary antibodies were used: peroxidase-coupled or CY5-coupled anti-mouse and anti-rabbit IgG (Jackson ImmunoResearch); fluorescently labeled anti-rabbit and anti-guinea-pig IgG (IRDye 680/800, Rockland Immunochemicals); and Alexa633-labeled anti-guinea-pig IgG and Alexa555-labeled anti-rabbit IgG (Invitrogen).

Generation of VGLUT1^{Venus} KI mice. The targeting vector was constructed on the basis of a 14 kb genomic clone of the *VGLUT1* locus in pBluescript, which had been isolated from a λFIXII genomic library of the SV129 mouse strain (Stratagene). In the targeting vector, the STOP codon in the last coding exon (exon 12) of the *VGLUT1* gene was replaced in-frame by a *venus-loxP-neo^r-loxP* cassette using recombineering techniques with engineered primers. The Venus cDNA was kindly provided by Dr. A. Miyawaki (RIKEN, Wako, Japan), and the recombineering toolbox was provided by Dr. N. Copeland (NCI, Frederick, MD). The *venus-loxP-neo^r-loxP* cassette was inserted between a 6.7 kb genomic sequence in 5′ position and a 7.9 kb genomic sequence in 3′ position (Fig. 1*C*). Mice carrying the mutated *VGLUT1^{VenusNeo}* gene (*VGLUT1$^{vn/+}$*) were generated by homologous recombination in embryonic stem cells (SV129/ola) as described previously (Thomas and Capecchi, 1987; Augustin et al., 1999) and identified by Southern blotting or PCR (Fig. 1*D*,*E*). To eliminate deleterious effects of the neomycin resistance gene, we crossed heterozygous VGLUT1$^{vn/+}$ mice with EIIa-cre mice that express Cre recombinase in early embryonic stages (Lakso et al., 1996). Successfully recombined *VGLUT1^{Venus}* alleles (v/+) in offspring from these interbreedings were genotyped by PCR (Fig. 1*D*). Except for initial comparative analyses of VGLUT1^{VenusNeo} and VGLUT1^{Venus} mice (Fig. 1), Cre recombined VGLUT1^{Venus} mice were used for all experiments. All experiments were performed with littermates derived from crossing heterozygous VGLUT1$^{v/+}$ or homozygous VGLUT1$^{v/v}$ mice (F2 SV129/ola × C57BL/6 genetic background). All live imaging experiments were performed on VGLUT1$^{v/v}$ mice. The probe used for embryonic stem (ES) cell screening by Southern blot was amplified from the *VGLUT1* locus. It is located on the mouse chromosome 7 contig NT_039424.7 at position 6081938–6082223. The following oligonucleotides were used for genotyping PCRs: 9420, CTGGCTGGCAGTGACGAAAG; 9421, CGCTCAGGCTAGAGGTGTATGGA; 9423, CTTCAAGATCCGCCACAACATCG; 4174, CGCATCGCCTTCTATCGCCTTCTT. Oligonucleotides 9420 and 9421 were used to amplify

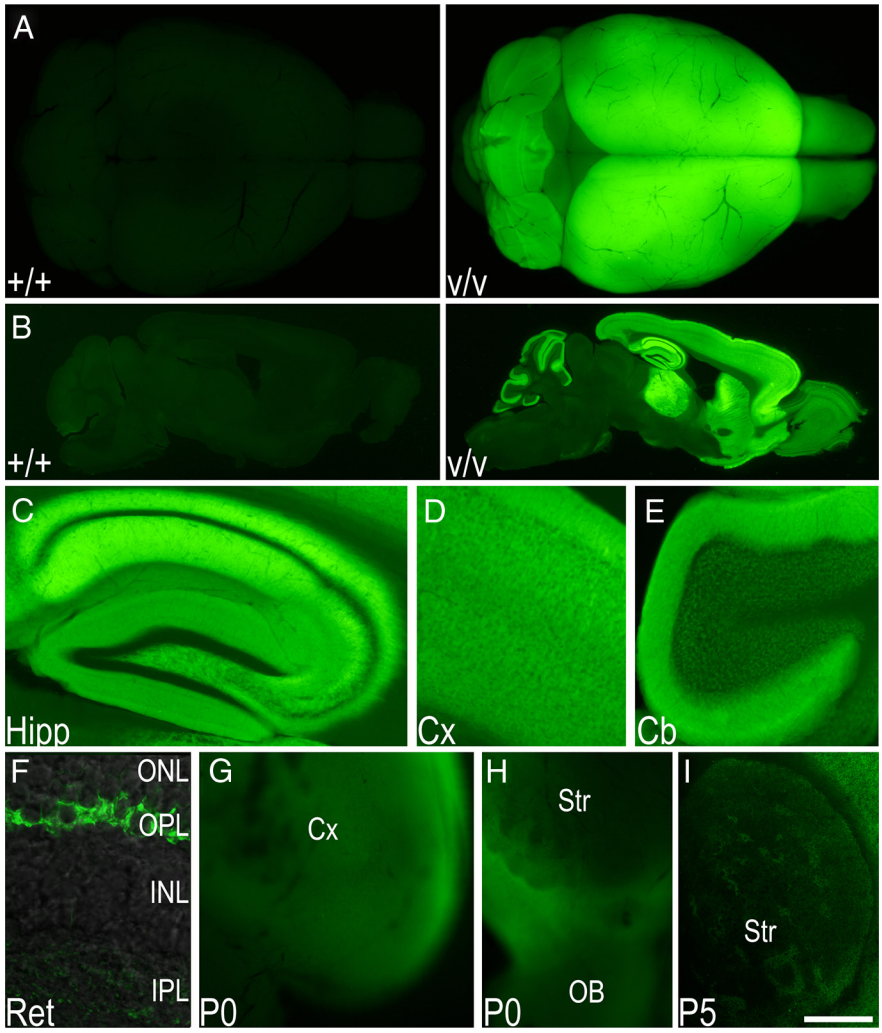

Figure 2. Regional and cellular localization of VGLUT1^{Venus} in the brain. ***A***, ***B***, Overview of direct VGLUT1^{Venus} fluorescence in paraformaldehyde-fixed +/+ and v/v mouse brains and sagittal sections. Scale bar, 2 mm. ***C–E***, Higher-resolution images of the v/v section shown in ***B*** depicting hippocampus (Hipp), cortex (Cx), and cerebellum (Cb). Fine puncta of fluorescent material, which are very similar to structures that are typically stained by conventional anti-VGLUT1 immunohistochemistry (Fig. 1*B*), are concentrated in neuropil areas. Scale bar, 500 μm. ***F***, High-resolution image of a v/v retina section. Bright VGLUT1^{Venus}-positive varicosities are found in the outer and inner plexiform layers (OPL, IPL), which contain glutamatergic ribbon synapses. Ret, Retina; ONL, outer nuclear layer; INL, inner nuclear layer. Scale bar, 20 μm. ***G***, ***H***, Newborn v/v brain (P0) at dorsal view (***G***) and ventral view (***H***). Note the lack of fluorescence in the striatum (Str). Scale bar, 500 μm. ***I***, Coronal section of a v/v brain at postnatal day 5 (P5) showing the striatum. VGLUT1^{Venus}-positive corticostriatal fibers enter the striatum preferentially through the striosomes. Scale bar, 700 μm.

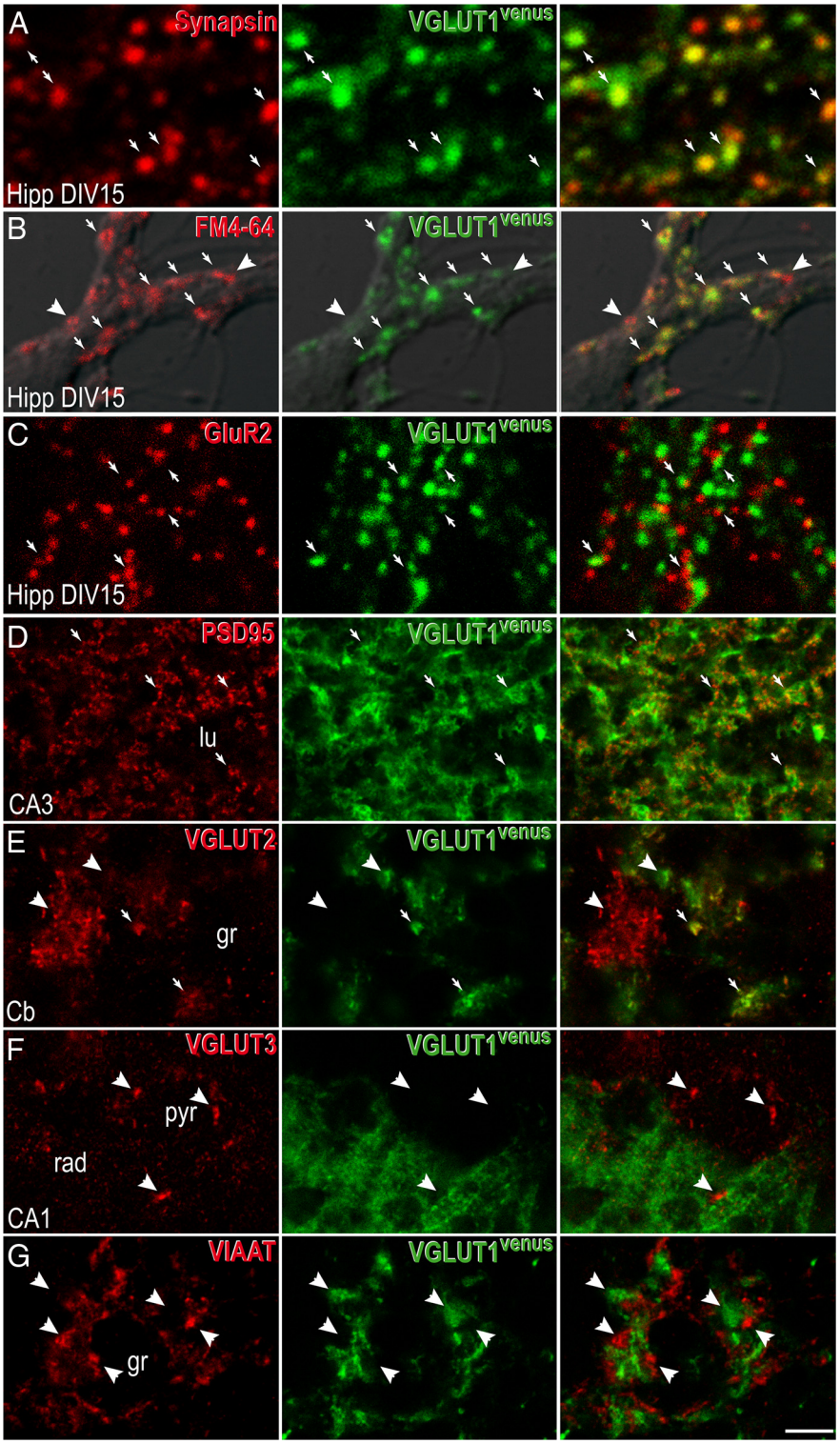

Figure 3. Subcellular localization of VGLUT1^{Venus}. ***A***, Colocalization of VGLUT1^{Venus} with SynapsinI/II in DIV15 cultured hippocampal neurons. Most VGluT1^{Venus} puncta colocalize with Synapsin-positive puncta (arrows), but their relative intensities vary. As expected some Synapsin-positive puncta do not contain VGLUT1^{Venus} and may represent inhibitory synapses. ***B***, Colocalization of VGLUT1^{Venus} with loaded FM4-64 (by KCl stimulation) in DIV15 cultured hippocampal neurons (arrows). As expected, some FM4-64-positive boutons do not contain VGLUT1^{Venus} (arrowheads) and may represent inhibitory synapses. ***C***, Apposition of VGLUT1^{Venus}-positive puncta and GluR2-positive clusters in DIV15 cultured hippocampal neurons (arrows). ***D***, Apposition of VGLUT1^{Venus}-positive puncta and PSD95-positive clusters in adult hippocampus CA3 stratum lucidum. Note patches of VGLUT1^{Venus} surrounded by small PSD95-positive puncta (arrows). ***E***, Partial colocalization of VGLUT1^{Venus}-positive structures and VGLUT2-positive mossy fiber terminals in adult cerebellum. As described previously (Hisano et al., 2002), VGLUT1 and VGLUT2 are partially segregated (arrowheads) and partially colocalized in some terminals (arrows). ***F***, VGLUT1^{Venus} and VGLUT3 are not colocalized in the CA1 area of the adult hippocampus (arrowheads). ***G***, Segregation of VGLUT1^{Venus}-positive structures and VIAAT-positive structures in glomeruli of the cerebellar granule cell layer (arrowheads). lu, Stratum lucidum; gr, granule cell layer; pyr, pyramidal cell layer. Scale bar (in ***G***): ***A***, 2 μm; ***B***, ***C***, 2.5 μm; ***D–F***, 10 μm; ***G***, 20 μm.

the WT *VGLUT1* allele, oligonucleotides 9421 and 9423 were used to amplify the *VGLUT1^{v}* allele, and oligonucleotides 9421 and 4174 were used to amplify the *VGLUT1^{vm}* allele.

Biochemical analyses. SDS-PAGE and Western blotting were performed according to standard procedures using HRP-coupled or IRDye 680/800-coupled secondary antibodies for qualitative or semiquantitative Western detection. Signals were either visualized on films by enhanced chemiluminescence (GE Healthcare) or scanned and quantified with the Odyssey imaging system (LI-COR Biosciences). Western blotting for VGLUT2 served as a loading control for VGLUT1^{Venus} quantification. Quantitative data are expressed as mean ± SEM. Subcellular fractionations were prepared essentially as described previously (Jones and Matus, 1974; Huttner et al., 1983). They were designated as follows: Hom, homogenate; P1, nuclear pellet; P2, crude synaptosomal pellet; SYN, sucrose gradient purified synaptosomes; LP1, lysed synaptosomal membranes; LP2, crude synaptic vesicle fraction; SPM, synaptic plasma membranes; S1, supernatant after nuclei sedimentation; LS1, supernatant after LP1 sedimentation; LS2, cytosolic synaptosomal fraction.

Histochemistry and immunofluorescence analyses. Direct VGLUT1^{venus} fluorescence and immunolabeling analyses were performed either on 40 μm cryotome sections cut from perfusion-fixed (4% paraformaldehyde), cryoprotected (30% sucrose) mouse brains or on fixed (4% paraformaldehyde) 15- to 21-d-old hippocampal primary neuron cultures. Samples were blocked and permeabilized (PBS, gelatin 2 g/L, 0.1% Triton X-100), and subsequently incubated with primary and secondary antibodies in the absence of Triton X-100. Extracellular immunolabeling for GluR2 was performed on live cultures by sequentially applying primary and secondary antibodies in culture medium through a perfusion chamber. Preparations were analyzed with an MZ16F epifluorescence stereo microscope or a TCS SP2 confocal laser-scanning microscope and corresponding software (Leica Microsystems).

Assays of vesicular glutamate uptake. Crude SVs (LP2 fraction) were prepared from VGLUT1$^{+/+}$ and VGLUT1$^{v/v}$ mouse brain cortices (as described above, in Biochemical analyses). Synaptic vesicles were then resuspended in 200 μl of ice-cold 0.32 M sucrose, 4 mM KCl, 4 mM $MgSO_4$, and 10 mM HEPES-KOH, pH 7.4 (uptake buffer). The transport reaction was started by addition of 10 μl of membranes (50 μg of protein) to 90 μl of uptake buffer containing 2.2 mM ATP-Mg, 44 μM glutamate, and 2 μCi [^{3}H]L-glutamate (PerkinElmer), with or without 55 μM carbonyl cyanide m-chlorophenylhydrazone (CCCP) and 5 μm Evans Blue. After incubation at 37°C for 10 min, [^{3}H] amino acid uptake was terminated by dilution with 3 ml of ice-cold uptake buffer, rapid filtration through a 0.45 μm pore size membrane filter (Millipore), and three washes with 3 ml of ice-cold uptake buffer. The radioactivity retained on the filters was measured by scin-

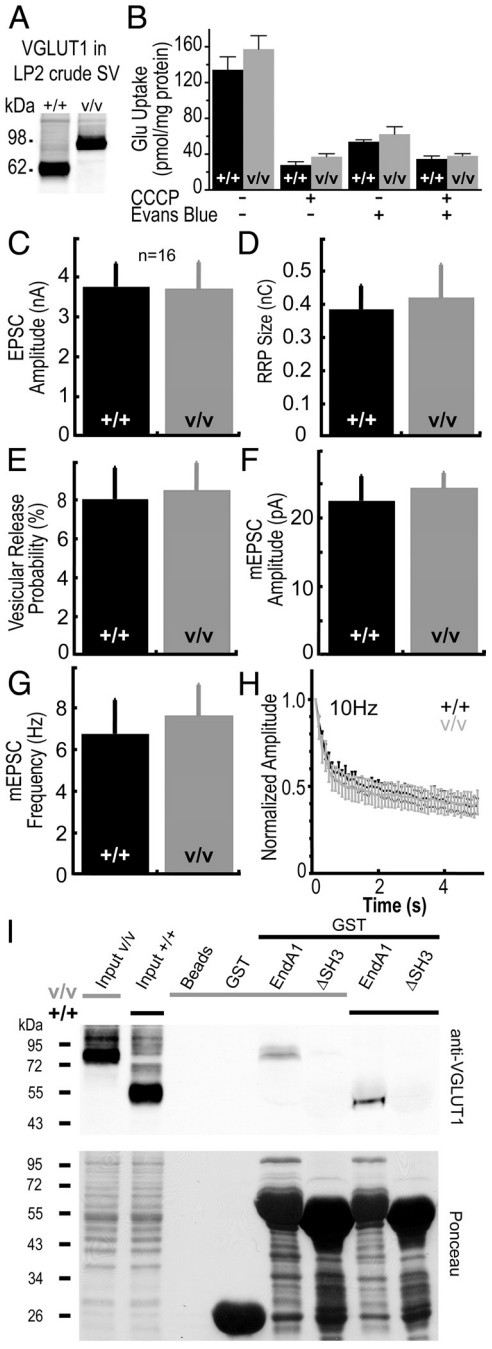

Figure 4. VGLUT1^{Venus} is a fully functional VGLUT1 transporter. ***A***, VGLUT1 and VGLUT1^{Venus} are expressed at similar levels in LP2 fractions used for vesicular uptake experiments. Western blot analyses of VGLUT1 expression showed a VGLUT1^{Venus}-positive band of the expected size (25 kDa larger than WT VGLUT1). ***B***, Glutamate uptake by VGLUT1^{Venus} and VGLUT1 SVs is similar (134.4 ± 28.8 pmol/mg protein for +/+ vs 157.4 ± 30 pmol/mg protein for v/v; $n = 4$). Glutamate uptake was abolished by the protonophore CCCP (27.9 ± 7.3 pmol/mg protein for +/+ and 37.3 ± 6.5 pmol/mg protein for v/v; $n = 4$) and by the specific VGLUT inhibitor Evans Blue (53.9 ± 3.8 pmol/mg protein for +/+ and 62.4 ± 14.2 pmol/mg protein for v/v; $n = 3$). ***C–H***, Synaptic transmission in VGLUT1^{Venus} neurons. Evoked EPSC amplitudes (***C***, $n = 16$), RRP size (***D***, $n = 13$), vesicular release probabilities (***E***, $n = 13$), mEPSC amplitudes (***F***, $n = 14$ for WT and $n = 8$ for v/v), mEPSC frequencies (***G***, $n = 14$ for WT and $n = 8$ for v/v), and synaptic depression during 10 Hz stimulation ($n = 13$) were identical in WT (+/+) and VGLUT1^{Venus} cells (v/v). Data are expressed as mean ± SEM. ***I***, Pull-down of VGLUT1^{Venus} and VGLUT1 from mouse brain homogenates using GST fusion proteins of EndophilinA1. Either full-length EndophilinA1 (EndA1) or a variant lacking the SH3 domain (ΔSH3) was fused to GST and used for pull-down of VGLUT1 variants from WT and v/v brain. Empty glutathione beads and GST alone served as additional negative controls. Load fractions and pull-down fractions were separated by SDS-PAGE and analyzed by Western blotting for VGLUT1. Note that only full-length EndophilinA1 coprecipitates VGLUT1 and that the WT and Venus-tagged carrier are pulled down with similar efficiency. The bottom panel shows the Ponceau S-stained blot to verify that comparable amounts of GST proteins were pulled down.

tillation counting in Ready Protein cocktail (Beckman). Each uptake measurement was performed in triplicate and is expressed as mean ± SEM. Experiments were independently performed three or more times. LP2 fractions used for uptake were monitored for the expression of VGLUT1 by Western blotting.

Glutathione-S-transferase pull-down assay. Glutathione-*S*-transferase (GST) pull-down assays were performed using the same constructs and protocols as described previously (Vinatier et al., 2006). Experiments were performed in parallel with WT and VGLUT1$^{v/v}$ brain tissues.

Electrophysiology and cell and tissue culture. Hippocampal autaptic microisland cultures were prepared as described previously (Pyott and Rosenmund, 2002) and examined using patch-clamp techniques according to previously published protocols (Rhee et al., 2002) at 12–16 d *in vitro* (DIV). Electrophysiological data are expressed as mean ± SEM and statistical significance of differences was determined using Student's *t* test. Mass neuron cultures for imaging experiments were prepared as for microisland cultures except that they were plated onto poly-L-lysine (Sigma-Aldrich)-coated coverslips at a density of 15,000 cells per cm^2. Imaging of live dissociated neuron cultures was performed at DIV16–21 in culture medium with added HEPES buffer (60 mM). Cycloheximide (20 μg/ml) exposure for 2 or 5 h and subsequent glutamate stimulation (2 h, 10 μM, after 2 h cycloheximide incubation) were performed on continental neuron cultures at DIV16–20, after which the neurons were fixed in 4% paraformaldehyde in PBS. Hippocampal slices were prepared from postnatal day 5–7 VGLUT1$^{v/v}$ mice according to published protocols (Gähwiler, 1981). In brief, slices were cut at 400 μm thickness, embedded in a plasma clot on glass coverslips, and incubated for 10–20 d at 35°C using the roller tube technique. Before the experiments, slice cultures were transferred into a recording chamber (35°C) and continuously perfused with artificial CSF (ACSF, 1 ml/min) containing 126 mM NaCl, 2.5 mM KCl, 2.5 mM $CaCl_2$, 1.3 mM $MgCl_2$, 20 mM glucose, 1.25 mM NaH_2PO_4, 26 mM $NaHCO_3$, 1 mM pyruvate, and 1 mM Trolox (Sigma). The temperature was maintained at 35°C, and the solution was continuously perfused with Carbogen (95% O_2, 5% CO_2) to maintain pH 7.4.

Image processing. Unless stated otherwise, all image processing was performed using the latest available version of ImageJ software together with the macbiophotonics plugins package (http://www.macbiophotonics.ca/).

In vitro *FRAP.* FRAP experiments were performed to determine the mobility of VGLUT1 at synapses. The mobile fraction of VGLUT1^{Venus} is defined by the proportion of fluorescent material that can be replenished after photobleaching. *In vitro* FRAP was performed on a Leica SP5 Laser Scanning Microscope using a 63×/1.32 numerical aperture oil-immersion objective and a thermal incubator set to 37°C surrounding the setup (Leica Microsystems). To enhance signal detection, the pinhole was opened to 2.5 Airy units. Randomly selected 41 μm^2 frames (512 × 512 pixels) were imaged with the 514 nm argon laser (power set to 80%, AOTF set to 2–4%) in 5 μm *Z*-stacks (eight steps per stack). From a test stack, five fluorescent boutons, distant from each other, were boxed for bleaching. Synapses were bleached by eight laser passes focused at the midplane of the stack using the 514 nm laser (AOTF at 100%) and the 405 nm diode laser (AOTF at 15%). This bleaching protocol prevents spontaneous recovery of Venus/EYFP fluorescence that has previously been reported (McAnaney et al., 2005) and ensured an average bleaching to 15% of the initial fluorescence of boutons. Fluorescence recovery was monitored every 30 s during the first 3 min and then every 5 min during the next 70 min. The entire FRAP procedure was automated using the SP5 live data mode software. The procedure was adapted for the double FRAP experiments with two bleaching steps and monitoring of recovery reduced to every 5 min. Image processing was automated using ImageJ macro commands. Sum projections of the individual stacks, assembly, and *x–y* realignment were applied, resulting in 32 bits/pixel sequences. Integrated fluorescence intensities of the five bleached and eight control

←

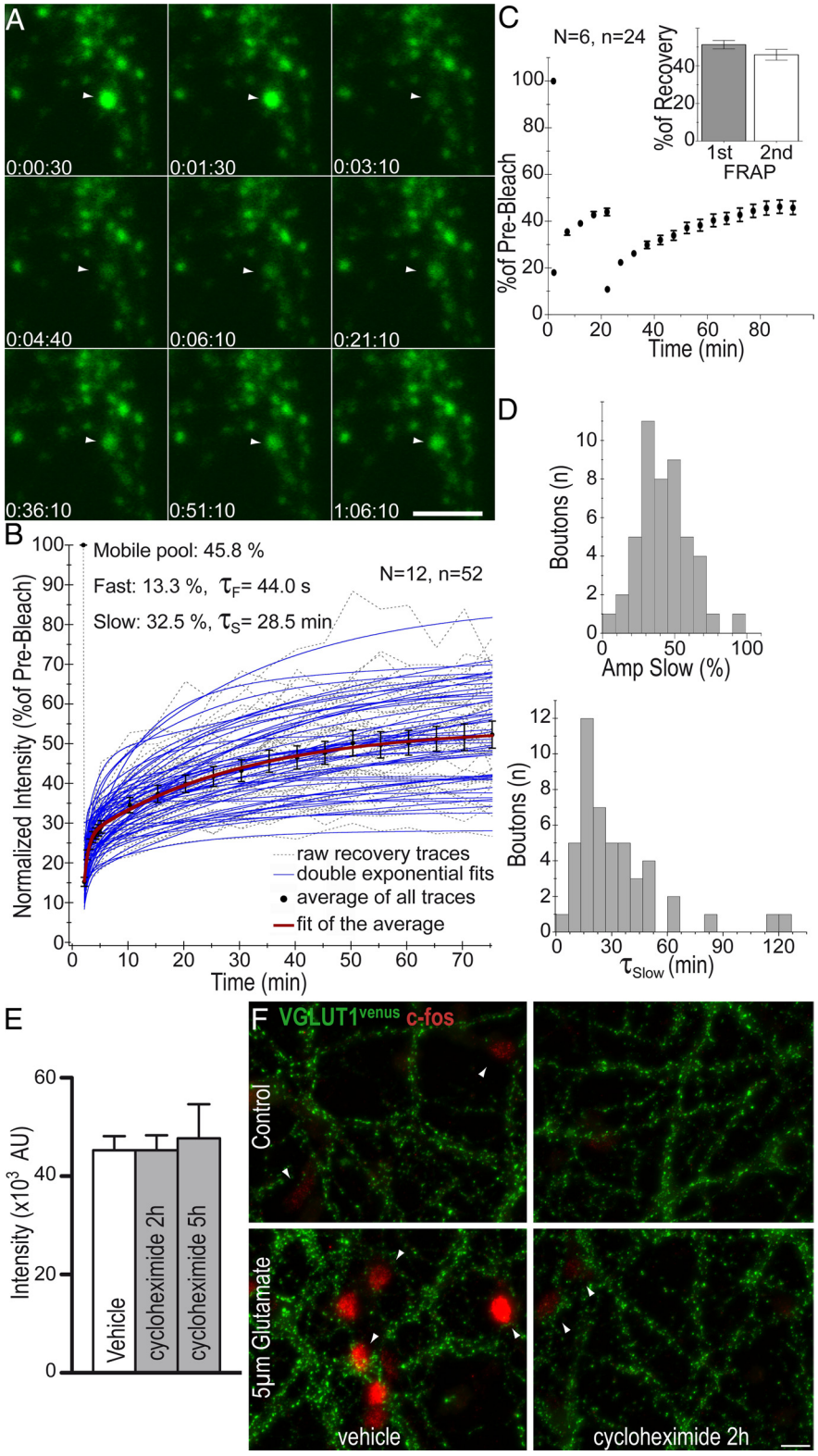

Figure 5. Mobility of VGLUT1^{Venus} measured by FRAP in synaptic boutons of neuron cultures. ***A***, Representative montage of a FRAP sequence. In randomly selected fields of the hippocampal neuron cultures, five stable fluorescent dots of at least 0.5 μm diameter were considered as synaptic boutons and selected for bleaching. Recovery was followed over 70 min. Note the incomplete recovery of fluorescence as compared to prebleach images. Scale bar, 5 μm. See also Movie 1. ***B***, Kinetics of VGLUT1^{Venus} FRAP in culture. VGLUT1^{Venus} FRAP displays a fast ($\tau_F = 44.0 \pm 6.2$ s; amplitude $A_F = 13.3 \pm 8\%$) and a slow ($\tau_S = 28.5 \pm 1.9$ min; $A_S = 32.5 \pm 4.1\%$) component and is incomplete within 70 min. Individual traces (dashed gray), average and SEM of individual traces (black), double exponential fits of individual traces (blue), and the double exponential fit of the average (red) are shown ($N = 12$ cultures, $n = 52$ boutons). ***C***, Double FRAP experiments. The average FRAP trace during double bleaching experiments is shown. A comparison of the amplitudes of recovery at 70 min after one or two bleaching steps is shown in the inset bar diagram. Note that FRAP is similar in both instances ($N = 6$ cultures, $n = 24$ boutons). ***D***, Distribution of time constants and amplitudes of the slow FRAP component. Parameters were calculated by fitting the individual traces displayed in ***B***. ***E***, Lack of influence of *de novo* protein synthesis on VGLUT1^{Venus} signals at boutons. Neuron cultures where incubated for 2 and 5 h with the translation inhibitor cycloheximide before fixation and quantification of fluorescence intensity at presynaptic boutons. Note that VGLUT1^{Venus} fluorescence intensity is unaffected by cycloheximide as compared to control cultures (3 cultures; $n = 20$ frames). ***F***, Potency of cycloheximide. To verify that the cycloheximide treatment was effective in our experiments, we examined its effect on c-fos synthesis. Expression of c-fos was induced by glutamate stimulation (10 μm, 2 h). Cycloheximide treatment abolished glutamate-induced c-fos expression (red) while VGLUT1^{Venus} fluorescence remained unaffected.

boutons as well as one background area were extracted. The background signal was subtracted, and data were normalized to the average baseline before bleaching and corrected for photobleaching against the average of the eight control varicosities. Experiments were discarded if unwanted photobleaching exceeded 20% of initial fluorescence before the end.

In vivo *FRAP experiments. In vivo* FRAP experiments (Fig. 6*A*) were performed with mice aged 8–12 weeks (weight range 20–35 g) under general anesthesia initiated by 60–80 mg of pentobarbital sodium intraperitoneally (dissolved in 0.9% NaCl solution) per kilogram of body weight. After cannulation of the jugular vein, the anesthesia was continued with 40–60 mg of methohexital sodium per kilogram of body weight (Brevimytal, Hikma). Then a tracheotomy was performed and a tracheal tube was inserted for artificial ventilation. The animal was paralyzed with pancuronium bromide (Pancuronium Organon, Essex Pharma) and artificially ventilated with a gas mixture of CO_2 (2.5%), O_2 (47.5%), and N_2 (50%) at 120 strokes/min (100–140 μl/stroke depending on the body weight). Layer I synapses from parietal cortex were imaged through the skull thinned with a dental drill (Fine Science Tools). For labeling of blood vessels, Texas Red-Dextran (70 kDa, 1.25% w/v, Invitrogen) was injected through an intravenous line placed in a tail vein. The mouse was given initially a bolus of 75 μl at 20 μl/min and was injected thereafter continuously at a slower rate (20 μl/h). The body temperature was measured rectally and kept between 36°C and 38°C by a heatable mouse support. Electrocardiograms were monitored throughout the experiment. For sufficient anesthesia, the heart rate was kept below 420 per minute, where surgical stress could not be detected any more. In addition to artificial ventilation, movements were attenuated by fixing the skull to the mouse support through a metal rod. Epifluorescence overviews of the cortex were acquired with a 5×/NA 0.15 objective (Carl Zeiss) and a CCD camera. High-resolution *in vivo* imaging was performed with a custom-made two-photon laser scanning microscope (2P-LSM) equipped

with an fs-pulsed, mode-locked titanium-sapphire infrared laser (Chameleon Ultra II; Coherent) and a Zeiss W Plan-Apochromat 20×/1.0 DIC water-immersion objective. The group velocity dispersion was precompensated (Chameleon PreComp Accessory, Coherent). The laser was set at 925 nm for the simultaneous excitation of VENUS and Texas Red. Emitted light was split by a 560 nm long-pass dichroic mirror (Semrock) and collected by photo-multiplier tubes (Hamamatsu) through a 510 ± 84 nm bandpass filter (Semrock) and a HQ575 long-pass filter (AHF Analysentechnik), respectively. The 2P-LSM was driven by ScanImage software (Version 3.1, Pologruto et al., 2003). For FRAP experiments, a few synapses with the highest signal were selected on single 30 × 30 μm^2 optical planes to be bleached or to serve as controls. Care was taken to choose planes containing vessels to provide coarse landmarks during the time lapse. Six images were recorded every 30 s. Then, the zoom factor was reduced to the size of a single synapse imaged with the same intensity at the same wavelength as the overall plane until no fluorescence was visible by eye. Typically, this required a few seconds whereas the remaining signal did not exceed 15% of the initial value. In case where bleaching was even faster, a second synapse was bleached. The overall plane was imaged immediately and again for 3.5 min every 30 s to assess the fast component of the recovery. Finally, images were taken every 5 min for 75 min to reduce ongoing bleaching. Despite the artificial respiration and the fixed skull, subtle movements (<1 μm/s) were still present. Thus, to be sure that the median plane of the synapses was detected reliably, they were imaged for each time point five times sequentially at the same height instead of obtaining a *z*-stack. The five intensities of each synapse were then averaged.

Time-lapse imaging of organotypic hippocampal slices. Time-lapse images from organotypic hippocampal slices were acquired using a custom-built two-photon laser scanning microscope. The excitation light from a Tsunami laser system (Coherent) was routed through a laser scan head (Yanus IV, TILL Photonics), a dichroic mirror (LOT Oriel), and a 40×, 1.2 NA water-immersion objective (Zeiss) mounted on an inverted IX70 microscope (Olympus). The Tsunami laser was used at a wavelength of 930 nm. The power of the excitation light was adjusted by an electro-optical modulator (Polytec) and kept constant during the experiments. The emitted fluorescence was split by a dichroic mirror (LOT Oriel) into red and green fluorescence, filtered by adequate bandpass filters (LOT Oriel), and detected by two external photomultiplier tubes (R6357, Hamamatsu). Image acquisition was performed by a custom-programmed software (LabVIEW 8.2, National Instruments).

Time-lapse imaging of cultured hippocampal neurons. Time-lapse sequences from cultured hippocampal neurons were collected using a Leica DMI6000 inverted microscope (Leica Microsystems) equipped with a Yokogawa CSU-X1 spinning disc confocal head (Roper Scientific) and a 100 mW 491 nm laser controlled by MetaMorph (Molecular Devices). The setup was enclosed in a thermal incubator set to 37°C. Images were collected through a 63×/1.4 numerical aperture oil-immersion objective and an additional 2× lens on a QuantEM:512SC EMCCD (Photometrics). Random fields of the cultures were selected and 3.2 μm stacks (5 steps) were acquired every 30 s for 1 h. Bleaching was <15% of initial fluorescence. Maximum intensity projections of the individual stacks, assembly, and *x–y* realignment were applied, resulting in 16 bits/pixel sequences. Maximum intensity projections of the entire sequence frames allowed an integrated view of boutons over 1 h. This projection was used to design 13 × 13 pixel boxes around sufficiently isolated boutons. Integrated fluorescence intensities of the boxed boutons as well as five background boxes were extracted from all frames and plotted in Excel. To monitor general bleaching due to acquisition, two larger 48 × 58 pixels boxes containing around 30 boutons were positioned around dense high-intensity areas and one on the background area. The background signal was subtracted and data were corrected for photobleaching using the average value measured in the two control boxes.

Imaging of fixed cultures. Images of fixed cultures (cycloheximide exposure experiments) were taken using a fully automated Zeiss Axiovert 200 fluorescence microscope with a 40× objective. Imaging parameters were determined once in the beginning for all acquisitions. For each condition, five locations were chosen randomly using neutral density filters to prevent bleaching as much as possible. Five frames were then imaged automatically in 3.2 μm stacks (five images per stack).

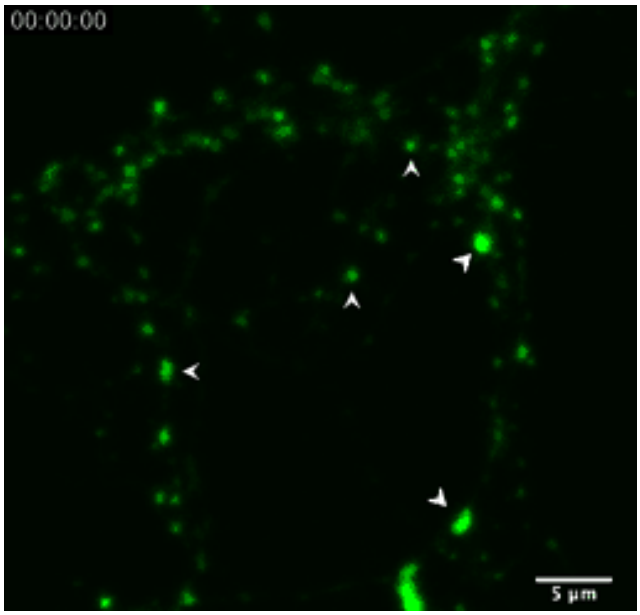

Movie 1. *In vitro* FRAP sequence related to Figure 5.

Analysis of in vivo *FRAP experiments.* The *x–y*-intensity profile of each synapse was first fitted with a two-dimensional symmetrical Gaussian curve. The diameter of the region of interest (ROI) was chosen as the full-width at half-maximum, which ranged between 4 and 6 pixels (430–650 nm). Next, the background, determined as the average of the lower intensities over all columns of the image, was subtracted from the intensity of the ROIs. Normalization was done in reference to the first six points before bleaching. Then, to correct for ongoing bleaching, the normalized intensities were divided by the normalized time profile of control ROIs. The final signal can thus be written as follows:

$$s = \frac{(I_{bl} - B)/\langle I_{bl}\rangle}{(I_{ctr} - B)/\langle I_{ctr}\rangle},$$

where I_{bl} is the time profile of the bleached ROI and $\langle I_{bl}\rangle$ its average over the six first points before bleaching. B is the time profile of the background. I_{ctr} represents the time profile of an unbleached synapse and is calculated as the average over a few control (unbleached) ROIs. $\langle I_{ctr}\rangle$ is the average of the latter over the six first points before bleaching. Synapses with <80% initial bleaching were discarded. Traces from single synapses were fitted with a double exponential function to reduce the noise due to experimental artifacts (mouse movement, low signal-to-noise ratio). This method was preferred to smoothing because it suppresses high-frequency variations (single aberrant points) without suppressing the fast component of recovery. Then, the average of all fitted curves was fitted with a double exponential function.

Analysis of in vitro *FRAP experiments.* Normalization was applied as for the *in vivo* data, but the smoothing fit was not necessary to reduce the noise. Rather, a double exponential function was used to fit the average of all normalized traces, and the parameters of the best fitting curve were considered as the parameters of a hypothetical average synapse. As a complementary approach, single traces were also fitted to extract the recovery parameters of each individual synapse to evaluate their distribution.

Analysis of time-lapse sequences. The analysis was intended to quantify the fluctuations in local VGLUT1^{Venus} levels of single synapses independently of their initial VGLUT1^{Venus} content, to represent their ability to modify their strength. Background subtracted time profiles of the fluorescence intensity measured on single synapses by the first 12 points (from 0 to 5.5 min) were normalized. These time profiles were mainly monotonic and linear with a few exceptions (Fig. 7*B*), the latter being

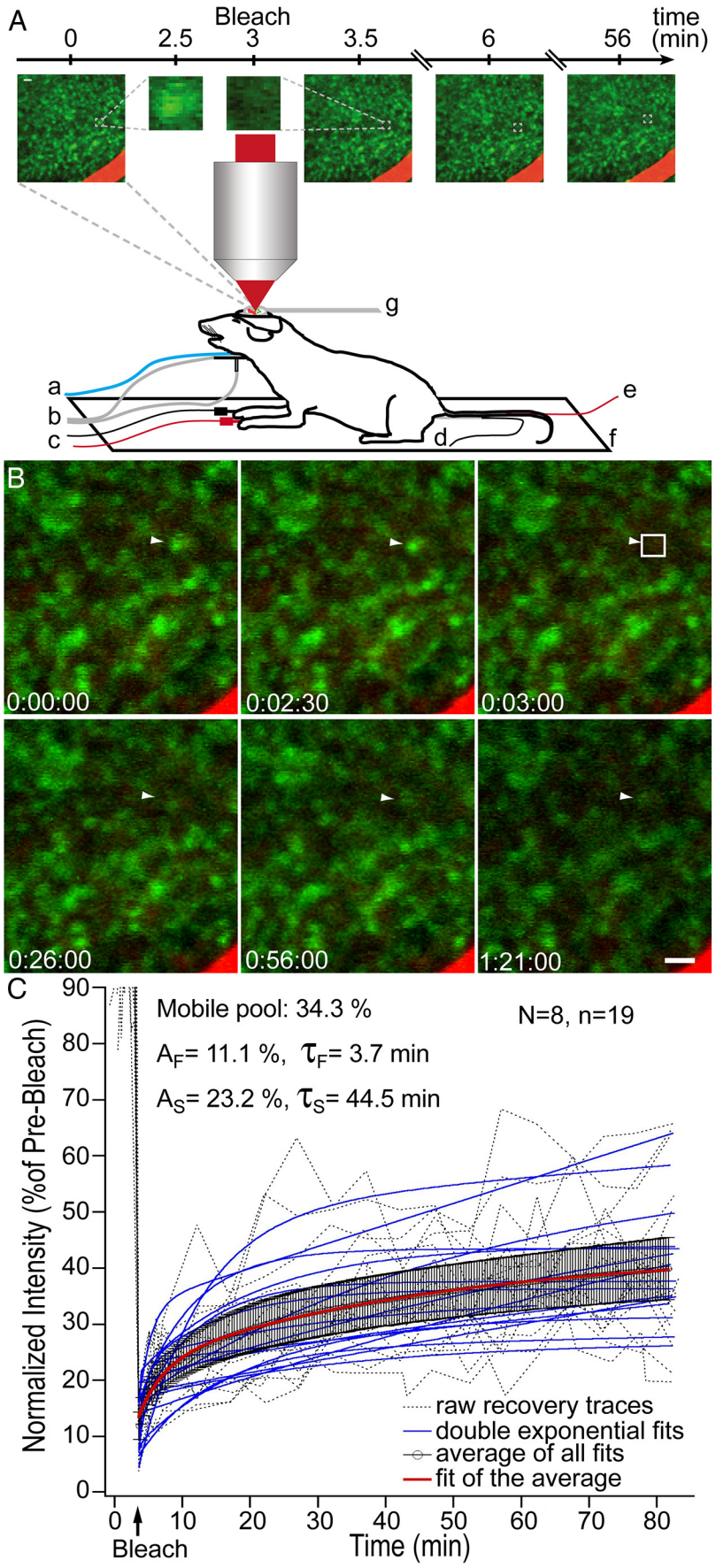

Figure 6. Mobility of VGLUT1^{venus} measured *in vivo* by FRAP in cortical synaptic boutons. ***A***, Experimental setup for *in vivo* FRAP imaging. The time line of the FRAP sequence was the same as for the *in vitro* experiments and was adapted to the constraints of the custom-built two-photon microscope. a, Intravenous line for anesthesia; b, tracheal tube for artificial ventilation; c, electrodes for electrocardiogram recording; d, rectal temperature measurement; e, intravenous line for the labeling of blood vessels; f, heating pad; g, metal rod for fixation. ***B***, Representative montage of a FRAP sequence performed in layer I of the anesthetized mouse cortex. Bright fluorescent puncta were selected for bleaching. FRAP was followed over at least 70 min. Note the lower degree of recovery compared to *in vitro* experiments (Fig. 4). Scale bar, 2 μm. See also Movie 1. ***C***, Kinetics of VGLUT1^{Venus} FRAP *in vivo*. VGLUT1^{Venus} recovery displays a fast ($\tau_F = 3.7 \pm 0.1$ min; amplitude $A_F = 11.1 \pm 0.3\%$) and a slow ($\tau_S = 44.5 \pm 1.3$ min; $A_S = 23.2 \pm 0.1\%$) component and is incomplete within 70 min. Individual traces (dashed gray), double exponential fits of individual traces (blue), average of double exponential fits with 95% confidence interval (black), and a double exponential fit of the average (red) are shown ($N = 8$ mice, $n = 19$ boutons).

characterized by the combination of a linear trend plus abrupt events (Fig. 8*C*). To have access to long-term (1 h timescale) fluctuations in local VGLUT1^{venus} levels regardless of the presence of a higher frequency component, the normalized curves were fitted with linear functions. Then, the calculated slope was compared to the arbitrarily chosen threshold of 10% intensity change per hour to classify synapses as exhibiting increasing, decreasing, or stable fluorescence levels. Finally the average curves for each type of synapse and the corresponding average intensity change rate were obtained by discarding from the distributions a few synapses with extreme outlier slopes.

Analysis of cycloheximide exposure experiments. Maximum intensity projections were generated from the acquired stacks (three cultures; $N = 20$ frames), the background was subtracted, and images were duplicated. One image was converted to 8 bit grayscale to allow single bouton identification using granulometric filters and thresholding. ROIs were saved and transferred to the original 16 bit images, where integrated intensity of fluorescence and area were then measured automatically. Average values for synapses of each frame were used for statistical comparison between cycloheximide and control conditions.

Results

Generation and characterization of VGLUT1^{Venus} KIs

Homozygous VGLUT1^{Venus} KIs carrying a Venus cDNA instead of the stop codon in exon 12 of the *VGLUT1* gene, followed by a neomycin resistance cassette in the 3′ untranslated region (vn/vn) were generated by homologous recombination in embryonic stem cells as described in Materials and Methods (Fig. 1*C*). To eliminate deleterious effects of the neomycin resistance cassette on VGLUT1^{Venus} expression (Fig. 1*F*), vn/+ mice were crossed with EIIa-cre mice, which carry the cre transgene under the control of the adenovirus EIIa promoter

and express Cre recombinase in early embryonic stages (Lakso et al., 1996). Mice carrying Cre recombined *VGLUT1^{Venus}* genes were bred to yield homozygous offspring lacking the neomycin resistance cassette (v/v) (Fig. 1*C*). Ninety-six ES cell clones were initially screened yielding 18 clones with the desired homologous recombination as identified by Southern blot analysis with a 3′ external probe (Fig. 1*D*). For routine breeding, PCR genotyping was performed (Fig. 1*E*). VGLUT1$^{v/v}$ animals are born at the expected Mendelian frequency and are indistinguishable from their WT and VGLUT1$^{v/+}$ littermates at birth. Neither VGLUT1$^{vn/vn}$ mice nor VGLUT1$^{v/v}$ mice showed any obvious behavioral or morphological alterations. They had a normal life expectancy and were fertile even when homozygous VGLUT1$^{v/v}$ animals were crossbred. This is in stark contrast to VGLUT1 KO mice, which display a severely perturbed phenotype in the third postnatal week and die ~18 d after birth (Wojcik et al., 2004). These observations already strongly support the notion that the Venus tag does not interfere with VGLUT1 function in VGLUT1$^{vn/vn}$ nor VGLUT1$^{v/v}$ mice. Nevertheless, we performed further thorough quantitative analyses of the neutrality of the KI mutation and the validity of the novel KI mouse model.

To assess the expression level of VGLUT1^{Venus} in the KI mice, WT and tagged transporters were systematically quantified in heterozygous and homozygous mouse brain homogenates by Western blotting with infrared fluorescence detection (Fig. 1*G*). In SDS-PAGE, Venus-tagged VGLUT1 migrates with the expected 25–30 kDa shift as compared to the WT protein and displays a slightly more compact migration profile. Quantification was performed by comparing normalized integrated intensities of both isoforms in the various genotypes. VGLUT2, which has a similar size, displays similar migration characteristics in SDS-PAGE, and is not aberrantly expressed in VGLUT1 KOs (Fremeau et al., 2004b; Wojcik et al., 2004), was used as an internal loading control for normalization (not shown). No differences were observed between VGLUT1 and VGLUT1^{Venus} expression, and a gene dosage effect was detected for both variants (0.54 ± 0.11 AU for VGLUT1^{venus} vs 0.53 ± 0.08 AU for VGLUT1, +/v, $n = 16$; 0.90 ± 0.11 AU, v/v, $n = 4$; 0.90 ± 0.08 AU, +/+, $n = 3$; Fig. 1*H*). Thus, in the mutant mice we generated, VGLUT1^{Venus} replaces VGLUT1 without upregulation or downregulation artifacts.

To further establish the proper expression and localization of VGLUT1^{Venus}, we analyzed subcellular fractionations of VGLUT1$^{v/+}$ mouse brains by Western blotting. We found WT VGLUT1 and VGLUT1^{Venus} to be distributed exactly in parallel in the different subcellular fractions with a clear enrichment in the LP2 fractions, which contain crude SVs. When probing with an anti-GFP antibody, which recognizes Venus, we detected a single diffuse band at ~92 kDa, which represents VGLUT1^{Venus} and was also enriched in the LP2 fraction. Thus, VGLUT1^{Venus} is normally targeted to SVs, in parallel with the SV marker Synaptophysin (Fig. 1*I*). Likewise, the developmental expression pattern of VGLUT1^{Venus} is identical to that of its WT counterpart as assessed by Western blot analyses of brain homogenates from mice ranging in age between postnatal days P0 and P110, where both variants show a parallel rise in expression starting around P3 and reaching a plateau at the climax of synaptogenesis around P21 (Fig. 1*J*).

Localization of Venus fluorescence in VGLUT1^{Venus} mouse brain

Paraformaldehyde-fixed VGLUT1^{Venus} brains display a bright and well defined fluorescence signal that was excited optimally at 514 nm and collected in the 520–560 nm range. Similar excitation and collection yielded a barely detectable background autofluorescence signal in WT brains (Fig. 2*A*,*B*). In sagittal brain sections, VGLUT1^{Venus} fluorescence is prominent in olfactory bulb, cortex, striatum, hippocampus, thalamus, and cerebellar cortex (Fig. 2*B*), all regions that are known to receive dense VGLUT1-positive innervation. Higher magnifications showed typical VGLUT1 labeling patterns in the neuropil of hippocampus, cortex, and cerebellum. As expected, no Venus signal was detected in the cell body layers (Fig. 2*C–E*; for comparison with immunofluorescence stainings, see Fig. 1*B*) (Bellocchio et al., 1998; Herzog et al., 2001; Kaneko et al., 2002). In the cortex, VGLUT1^{Venus} fluorescence is already detectable at birth (Fig. 2*G*), which is not the case in the striatum (Fig. 2*H*), whose innervation by corticostriatal glutamatergic fibers begins at postnatal day 4 (Fig. 2*I*) (Boulland et al., 2004). In the retina, VGLUT1^{Venus} was detected in the outer and inner plexiform layers, which are typical VGLUT1-containing regions (Fig. 2*F*) (Mimura et al., 2002). Further colocalization studies showed a normal association of VGLUT1^{Venus} fluorescence with presynaptic markers and an apposition to typical glutamatergic postsynapse markers (Fig. 3*A–D*). No aberrant overlap of VGLUT1^{Venus} fluorescence was seen with VGLUT2-, VGLUT3-, or VIAAT-immunopositive structures (Fig. 3*E–G*). We next used two-photon microscopic analyses of organotypic hippocampal slices from VGLUT1^{Venus} mice. To test whether VGLUT1^{Venus} puncta colocalize with axons and axonal varicosities, we colabeled Schaffer collaterals by loading of single CA3 neurons with a morphological tracer dye via a patch pipette and found that morphologically identified boutons selectively colocalized with VGLUT1^{Venus} puncta (data not shown).

Together, the above morphological observations demonstrate that the Venus tag does not interfere with the spatiotemporal expression pattern and subcellular localization of VGLUT1^{Venus}. It is properly targeted to excitatory presynaptic terminals and its distribution in brain is indistinguishable from that of WT VGLUT1.

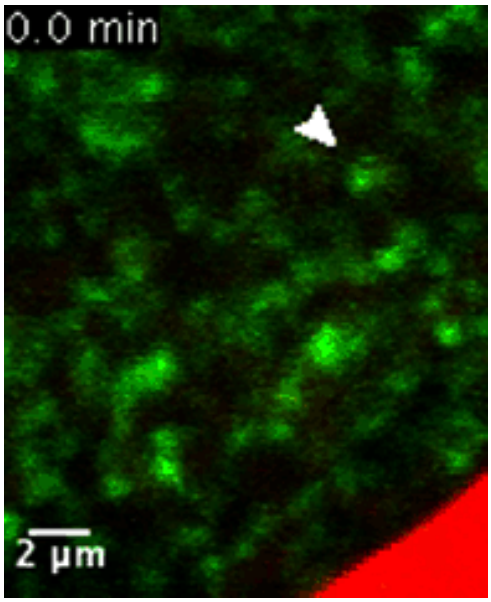

Movie 2. *In vivo* FRAP sequence related to Figure 6.

Functional characterization of VGLUT1^{Venus}

Before the establishment of the VGLUT1^{Venus} KI, we had used Semliki Forest viruses expressing VGLUT1^{Venus} to successfully recover a

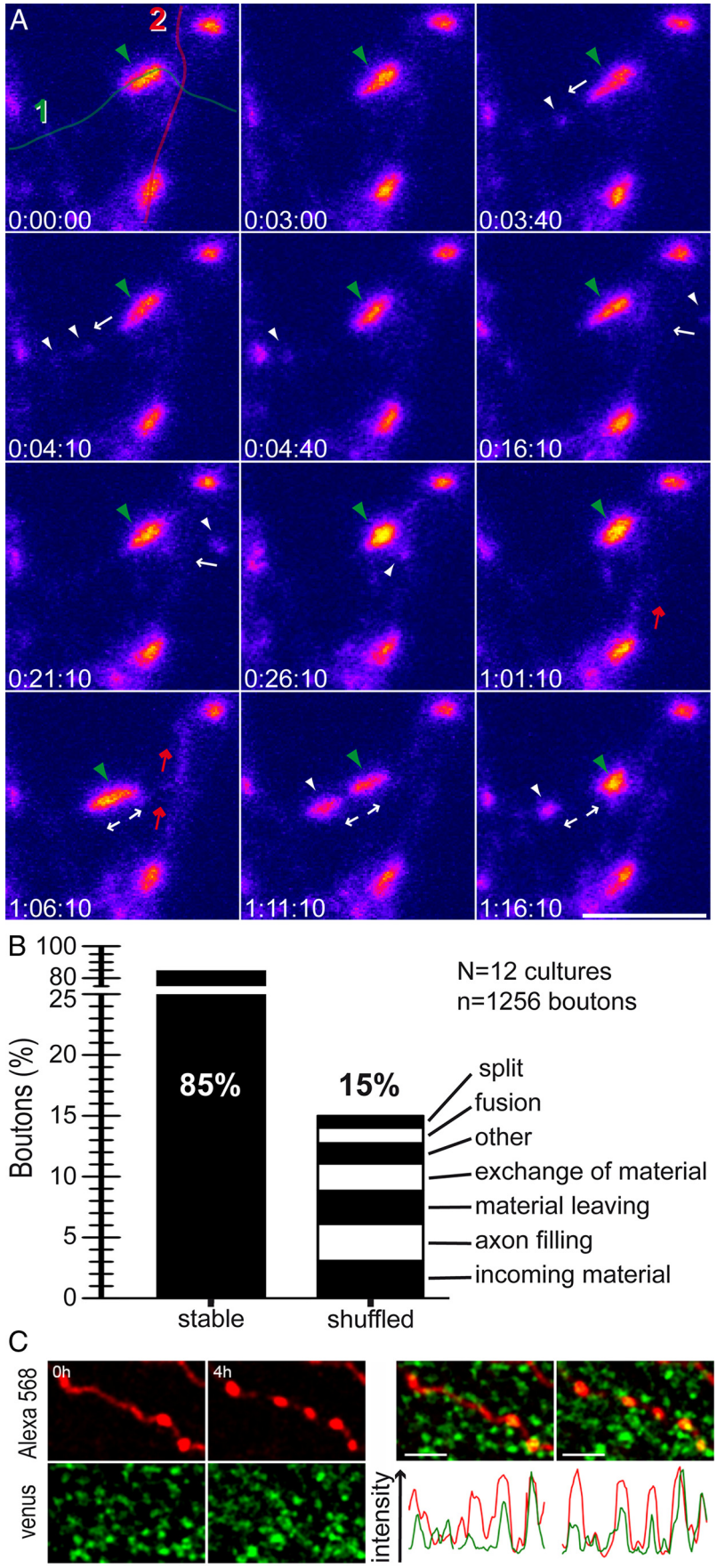

Figure 7. Analysis of large fluorescence changes in VGLUT1^{Venus}-positive presynaptic boutons. ***A***, Examples of boutons undergoing discontinuous shuffling of their VGLUT1^{Venus} content during the FRAP sequences analyzed in Figure 5 (see also Movie 3). Two axonal fibers (green and red lines) were identified. Tracking of fluorescent material was performed over 75 min (note that the sampling rate over time was not constant). Between 0 and 20 min, transit of fluorescent small clusters is seen in fiber 1 (white arrows and arrowheads). At 1 h, fiber 2 is filled by a flow of fluorescent material (red arrows). At the end of the experiment, a large cluster of VGLUT1^{Venus}-positive material is detached (white arrows) from the main bouton in fiber 1 (green arrowhead). Scale bar, 5 μm. ***B***, Quantification of the occurrence of stable versus changing boutons in the FRAP sequences. Discontinuous large events were sorted into the indicated categories. ***C***, VGLUT1^{Venus} associates with newly formed axonal varicosities. CA3 cells from cultured hippocampal slices of v/v mice were patch-filled with Alexa 568 and time-lapse imaging of morphological plasticity of axonal varicosities and VGLUT1^{Venus} content was performed. The images depicted here show examples of two new axonal varicosities that are positive for VGLUT1^{Venus} 4 h after their formation. Top left, Alexa 568-labeled axons; bottom left, VGLUT1^{Venus} fluorescence, top right, overlay. The plot at the bottom right depicts the fluorescence intensity profiles of Alexa 568 (red) and VGLUT1^{Venus} (green) along the axon. Scale bar, 5 μm.

WT-like phenotype in VGLUT1 KO neurons, which are characterized by a severe deficit in glutamate release [the effectivity of VGLUT1^{Venus} to rescue the VGLUT1 KO phenotype is shown by Wojcik et al. (2004), but the identity of the rescue construct as VGLUT1^{Venus} is not explicitly stated in the corresponding methods information]. Vesicular glutamate uptake activity of VGLUT1^{Venus} was measured using crude SVs (LP2 fractions) from VGLUT1$^{v/v}$ mice and compared to that of VGLUT1$^{+/+}$ SVs (Fig. 4*A*,*B*). VGLUT1^{Venus} and VGLUT1 were expressed at similar levels in the LP2 fractions assayed and transported glutamate similarly in a proton gradient-dependent manner (134.4 ± 28.8 pmol/mg protein for VGLUT1 vs 157.4 ± 30 pmol/mg protein for VGLUT1^{Venus}; $n = 4$). This specific uptake was abolished by Evans Blue, a competitive inhibitor of VGLUTs (53.9 ± 3.8 pmol/mg protein for VGLUT1 vs 62.4 ± 14.2 pmol/mg protein for VGLUT1^{Venus}; $n = 3$; Fig. 4*B*). These experiments indicate that VGLUT1^{Venus} in VGLUT1$^{v/v}$ mice has the same intrinsic glutamate uptake characteristics as VGLUT1 in WT mice.

To further validate the normal function of VGLUT1^{Venus} in our KI mouse model, we compared synaptic transmission characteristics of VGLUT1^{Venus} and WT neurons in autaptic culture, a preparation that we had used previously for a characterization of VGLUT1 KO neurons (Wojcik et al., 2004). EPSC amplitudes evoked by 2 ms depolarizations at 0.2 Hz were identical in VGLUT1^{Venus} (3.65 ± 0.67 nA; $n = 16$) and WT neurons (3.71 ±

0.58 nA; $n = 16$) (Fig. 4*C*). Likewise, the size of the primed, readily releasable pool (RRP) of vesicles, as assessed by integrating the total charge transfer of the transient component of the EPSC response during the pulsed application (5 s) of a hypertonic extracellular solution containing 0.5 M sucrose to the entire cell (Rosenmund and Stevens, 1996), was indistinguishable between VGLUT1^{Venus} (0.41 ± 0.10 nC; $n = 13$) and WT (0.38 ± 0.07 nC; $n = 13$) neurons (Fig. 4*D*). We calculated the vesicular release probability P_{vr} for the neurons analyzed by determining the ratio of the charge transfer during an evoked EPSC and the charge transfer elicited by release of the entire RRP during the application of hypertonic sucrose solution. As predicted from the evoked EPSC and RRP measurements, P_{vr} values for VGLUT1^{Venus} neurons (8.4 ± 1.4%; $n = 13$) and WT control cells (8.0 ± 1.6%; $n = 13$) were very similar (Fig. 4*E*). Likewise, the amplitudes and frequencies of miniature EPSCs were not different between VGLUT1^{Venus} (24.2 ± 2.2 pA; 7.6 ± 1.5 Hz; $n = 8$) and WT (22.3 ± 3.6 pA; 6.7 ± 1.6 Hz; $n = 14$) neurons (Fig. 4*F*,*G*), and upon 10 Hz stimulation, evoked EPSCs depressed exactly in parallel in VGLUT1^{Venus} and WT cells ($n = 13$). These electrophysiological data demonstrate that synaptic vesicle loading and transmitter release are not affected by the Venus tag on VGLUT1 in the KI mutant.

In a final set of validation experiments, we examined the ability of VGLUT1^{Venus} to bind one of its key interaction partners, EndophilinA1, which binds to a very C-terminal proline-rich motif of VGLUT1 (Vinatier et al., 2006). This interaction was previously shown to influence the recycling of VGLUT1-containing SVs (Voglmaier et al., 2006) and expected to be unchanged in VGLUT1^{Venus} based on the electrophysiological data described above (Fig. 4*C–G*). We performed GST pull-down experiments to compare the ability of WT and Venus-tagged VGLUT1 to interact with a GST-EndophilinA1 fusion protein, and detected no differences between the two VGLUT1 variants (Fig. 4*H*).

Together, the functional validation data described above together with our morphological analyses of the expression and subcellular distribution of VGLUT1^{Venus} demonstrate that VGLUT1^{Venus} is a fully functional fluorescent VGLUT1 variant with WT-like characteristics and that the KI mutation we introduced did not cause any unwanted collateral effects on the function of glutamatergic synapses.

VGLUT1^{Venus} turnover in presynaptic boutons of cultured hippocampal neurons

In a first approach to employ the new VGLUT1^{Venus} KI mouse model for the examination of SV trafficking characteristics, we used DIV16–21 hippocampal neuron cultures to assess SV mobility by FRAP analyses with the aim to determine the exchange of bleached SVs with fluorescent extrasynaptic SVs (Fig. 5, Movie 1). Bleaching stimuli were applied to selected stable presynaptic boutons, and fluorescence recovery was monitored in two phases for 70 min in total (Fig. 5*A*,*B*). During the first 3 min of recovery, stacks were acquired every 30 s, ensuring reliable sampling of fast events. As this sampling rate induces a significant bleaching, the sampling rate was subsequently reduced to one stack per 5 min in the following phase. A minor proportion of experiments leading to >20% bleaching due to acquisition were rejected. In all other cases, a correction for photobleaching was applied during data processing.

Bleached boutons displayed a robust but incomplete recovery of fluorescence over 1 h of observation (Fig. 5*B*). Quantitative analyses of fluorescence recovery showed that boutons harbor on

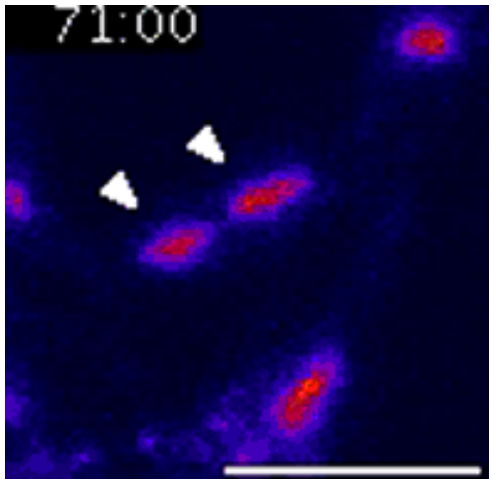

Movie 3. Time-lapse sequence related to Figure 7.

average a mobile SV fraction of 46% as assessed by VGLUT1^{Venus} fluorescence recovery (45.8 ± 4%; $N = 12$ cells, $n = 52$), with the remaining 54% of VGLUT1^{Venus}-positive structures being immobile at this timescale (54.2 ± 4%, $N = 12$ cells, $n = 52$; Fig. 5*B*). To ensure that these observations were not confounded by phototoxicity, we performed double FRAP experiments, where a second bleaching stimulus was applied 20 min after the first and recoveries monitored with one stack every 5 min. Recovery amplitudes after the second bleaching stimulus were similar to the ones observed in single FRAP experiments, indicating that presynaptic boutons indeed contain a mobile and a stable pool of VGLUT1^{Venus}-positive SVs (Fig. 5*C*).

The best fit of the average FRAP curve was achieved with a biexponential function. The initial component of recovery was rather fast with a τ_F of 44.0 ± 6.2 s ($N = 12$ cells, $n = 52$ boutons) and an amplitude A_F of 13.3 ± 8% of the prebleach VGLUT1^{Venus} fluorescence of the boutons. The slow FRAP component had a τ_S of 28.5 ± 1.9 min and an amplitude A_F of 32.5 ± 4.1% ($N = 12$ cells, $n = 52$ boutons) (Fig. 5*B*). The initial fast phase of FRAP recovery likely reflects the fast axonal transport of SVs to bleached boutons and the exchange of bleached SVs that are loosely associated with SV clusters, while the slow FRAP phase may represent exchange of bleached clustered SVs with the axonal SVs (Darcy et al., 2006). To examine whether the 52 observed boutons behaved in a similar way or rather correspond to distinct populations, we fitted individual recovery traces (Fig. 5*B*, blue lines) and displayed the distribution of their τ_S and amplitude (Fig. 5*D*; data for fast FRAP component were similar to those of the slow component and are therefore not shown). The frequency distributions of the corresponding values showed a single peak, indicating that the boutons assayed in our experiments do not represent multiple populations with regard to their VGLUT1^{Venus} FRAP characteristics.

In a set of control experiments, we examined the contribution of *de novo* protein synthesis to the turnover of VGLUT1^{Venus} at presynapses. To that end, we treated hippocampal cultures at DIV16–21 with the translation inhibitor cycloheximide (20 μM) for 2 or 5 h before fixation. VGLUT1^{Venus} fluorescence levels at boutons were then measured and compared to data from cells treated with vehicle only. No significant effect of translation inhibition was detected at this timescale (Fig. 5*E*,*F*). To verify that the cycloheximide treatment was effective in principle, we tested for the inhibition of c-fos expression by the same dose of cycloheximide applied for 2 h upon induction of c-fos expression by bath application of glutamate

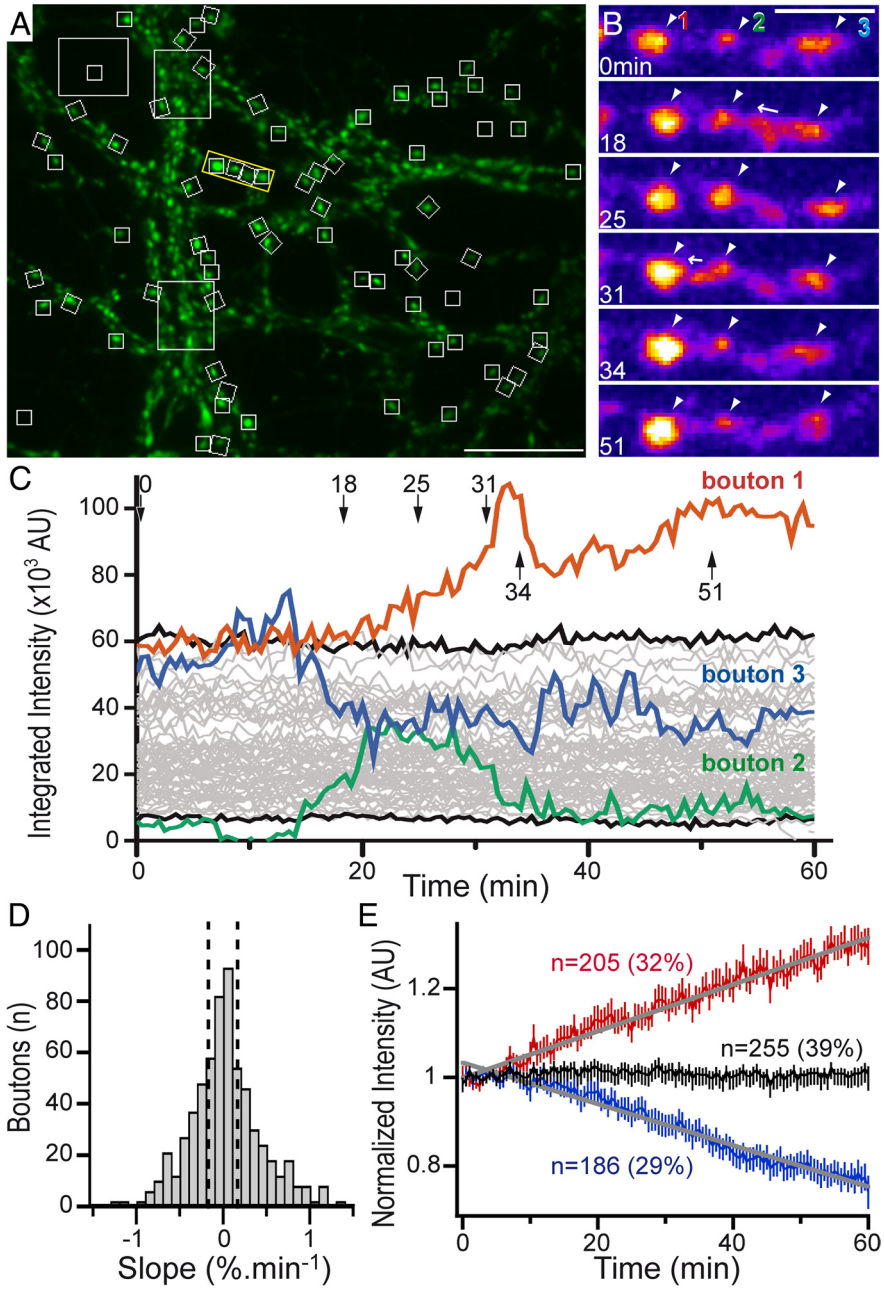

Figure 8. Exchange of SVs and fluctuations of SV content in synapses. ***A***, Representative frame imaged for 1 h every 30 s. The image shows a maximum intensity projection that was used to define isolated static boutons for quantification (small white boxes). Larger boxes depict areas used for monitoring unwanted bleaching. Three boutons are magnified in ***B*** (yellow box). Scale bar, 20 μm. See also Movie 4. ***B***, Transit of VGLUT1^{Venus} and shifts in fluorescence intensities among three synapses. Bouton 3 loses material that passes through bouton 2 to enter bouton 1 (arrows). Scale bar, 5 μm. ***C***, VGLUT1^{Venus} intensity plot of the time-lapse experiment displayed in ***A*** and ***B***. The traces corresponding to the three boutons depicted in ***B*** are colored correspondingly. Note the tight correlation between loss and gain of material among the three boutons. The black traces depict two examples of boutons with stable intensity. Six hundred forty-six time-lapse curves from isolated boutons (8 fields, 3 cultures) were recorded, normalized to time 0, and linear fits of these curves were generated. AU, Arbitrary units. Arrows show time points displayed in ***B***. ***D***, Changes in VGLUT1^{Venus} intensity during 1 h. The distribution of the slopes of linear fits extracted from the 646 recorded bouton intensity traces is shown. Note the Gaussian distribution around a mean slope value of 0, which represents boutons with stable intensity. Curves were then sorted into three pools of boutons (>10% gain of fluorescence, no change, >10% loss of fluorescence). ***E***, Average curves for boutons categorized as described for ***D***. Overall, 32% of boutons gained ~30% of VGLUT1^{Venus} within 1 h, with an average rate of change in the range of 0.5%/min ± 0.007%/min, while 29% of boutons lost ~30% of their VGLUT1^{Venus} content at the same rate. In ~39% of boutons, changes were balanced so that they maintained their VGLUT1^{Venus} content.

(10 μM). While no effect of cycloheximide was detected in the Venus channel under these conditions, a strong inhibition of c-fos induction was readily detectable (Fig. 5*F*). Thus, changes in VGLUT1^{Venus} synthesis do not contribute significantly to the changes in VGLUT1^{Venus} levels in our FRAP experiments.

In vivo FRAP on VGLUT1-positive SVs in presynaptic boutons of the cerebral cortex

To test whether the characteristics of VGLUT1^{Venus} turnover that we measured *in vitro* reflect the actual physiological situation *in vivo*, we examined the mobility of VGLUT1^{Venus}-positive SVs *in vivo* by performing two-photon laser scanning microscopic analyses of the cerebral cortex of anesthetized mice. Mice were ventilated and kept at 37°C for the entire duration of the experiment, including surgery. Images were acquired in cortical layer I through the thinned scull to ensure maximal intensity and resolution (see experimental setup in Fig. 6*A*). FRAP imaging was performed as described for experiments on hippocampal neuron cultures. The FRAP characteristics of VGLUT1^{Venus}-positive structures *in vivo* were very similar to those measured *in vitro* (Fig. 6*B*, Movie 2). Quantification of recovery kinetics of 19 boutons from 9 mice confirmed an incomplete recovery with a smaller mobile fraction (34.3 ± 5.5%) than hippocampal nerve cell boutons in culture (45.8 ± 4%). Fitting of the average FRAP traces yielded a fast (τ_F = 3.7 ± 0.1 min; A_F = 11.1 ± 0.3%) and a slow (τ_S = 44.5 ± 1.3 min; A_S = 23.2 ± 0.1%) component. Interestingly, the time constants measured *in vivo* were somewhat slower than those measured *in vitro*, and the amplitude of the slow component was reduced in cortical boutons *in vivo*. Thus, cortical synapses *in vivo* contain substantially fewer mobile VGLUT1^{Venus}-positive SVs than synapses of cultured neurons.

Analysis of discontinuous movements of VGLUT1^{Venus}-positive organelles

During our FRAP analysis of cultured neurons, we observed multiple presynaptic boutons and fibers that underwent very strong and sudden changes of their VGLUT1^{Venus} content (see Movie 1 left side). Consequently, several bleached boutons had to be excluded from our analysis of continuous recovery curves because they exhibited very strong and discontinuous changes of fluorescence. To assess this phenomenon in more detail,

we systematically observed all boutons during *in vitro* FRAP experiments, determined whether they underwent discontinuous alterations, and classified them according to the type of change as (1) fusion of two boutons, (2) splitting up of one bouton into two, (3) large cluster leaving a bouton, (4) large cluster fusing with a bouton, (5) exchange of a cluster between boutons, (6) axon filling, and (7) other. Examples of these events are shown in Figure 7*A* and Movie 3. Here, the two fibers identified in the frame display a variety of these behaviors. In most cases, axons and associated boutons exhibited a combination of modes of VGLUT1^{Venus} SV exchange, such as continuous influx and efflux of material at a bouton, compatible in extent with the variations observed in individual FRAP traces, followed by splitting up into two daughter boutons (Fig. 7*A*, green), or axonal fibers with steady fluorescence over extended time periods that are transiently flooded with VGLUT1^{Venus}-positive SVs and subsequently return to their initial state (Fig. 7*A*, red). Altogether, we assayed 1256 boutons in 12 independent cultures. Among these, 189 (15%) showed strong discontinuous alterations of their VGLUT1^{Venus} content (Fig. 7*B*).

In addition, we performed time-lapse two-photon imaging experiments on organotypic hippocampal slices of VGLUT1^{Venus} mice. We filled individual CA3 pyramidal neurons with Alexa 568 via a patch pipette to visualize their axonal projections, the Schaffer collaterals. In labeled axonal fibers, *en passant* boutons, which likely reflect functional synapses, consistently colocalized with VGLUT1^{Venus}, and this colocalization remained largely stable for the entire duration of the experiment (4 h). Only in some cases did we observe VGLUT1^{Venus} puncta that appeared, disappeared, or changed their intensity over time. As illustrated in Figure 7*C*, we also detected VGLUT1^{Venus} puncta appearing within newly formed boutons, indicating an acute accumulation of VGLUT1-positive SVs in newly generated synapses.

Monitoring of VGLUT1^{Venus} levels at presynaptic boutons over time

The experiments described above indicate that VGLUT1^{Venus}-positive SVs are dynamically trafficked along axons and exchanged between synapses. This, in turn, is expected to cause fluctuations in local VGLUT1^{Venus} levels at synapses over time. To quantify such fluctuations, we performed 1 h time-lapse imaging of boutons at high sampling rates using a spinning disk confocal microscope (120 stacks/h). Eight such sequences from randomly selected frames of three independent DIV17–18 hippocampal cultures were acquired (Fig. 8*A–E*, Movie 4). All well defined boutons were boxed manually for quantification (Fig. 8*A*, see also Materials and Methods). For 646 selected boutons, integrated intensities corrected for background and bleaching were extracted for all time points and plotted (Fig. 8*C*, Movie 4).

The assayed boutons displayed substantial heterogeneity with respect to changes of fluorescence intensity. While some 39% were stable in the course of the experiment, independently of their initial fluorescence intensity, the remaining 61% displayed substantial increases or decreases of their VGLUT1^{Venus} content (Fig. 8). The type and extent of these changes were compatible with the FRAP data we obtained *in vitro* and *in vivo*.

We fitted the 646 individual time-lapse fluorescence traces with linear functions to categorize the fluorescence characteristics as increasing, decreasing, or stable over time. The slopes of these fits showed a Gaussian distribution around an average of 0 (Fig. 8*D*), which represents stable boutons that balance their gain and loss of VGLUT1^{Venus} over time. Using a slope of ±0.16%/min (±10%/h change) as a threshold, we categorized 186 boutons with decreasing VGLUT1^{Venus} content, 205 boutons with increasing VGLUT1^{Venus} content, and 255 stable boutons (Fig. 8*E*), and then calculated the averages of the raw traces within each of the three groups. The average traces of fluorescence change had a linear profile and the rate of change was similar in boutons with increasing or decreasing VGLUT1^{Venus} content (0.5%/min), which indicates that the same basic trafficking process causes SVs to enter or leave presynaptic boutons over time. Together, above data show that a large proportion of VGLUT1-positive presynaptic boutons alter their SV content by ~25–30% within 1 h. At the network scale, this exchange of VGLUT1^{Venus} SVs is unlikely to result in altered overall availability of glutamate-filled SVs, because the total VGLUT1 content does not seem to change as overall VGLUT1 gains and losses at synapses appear to be in balance (Fig. 8*E*). Nevertheless, the changes in VGLUT1 content that we observed occur in a large population of synapses and are substantial. This type of redistribution is likely to participate in regulatory processes that determine synapse strength and information coding in synaptic networks.

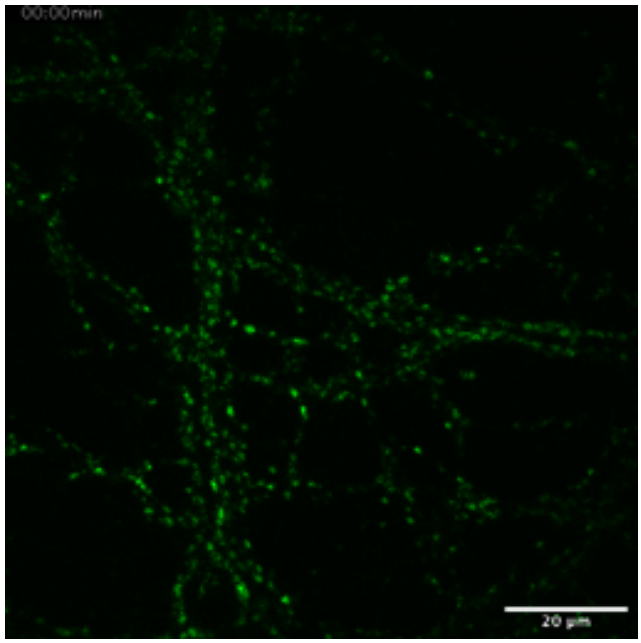

Movie 4. Time-lapse sequence related to Figure 8.

Discussion

We generated a VGLUT1^{Venus} KI mouse model for the live imaging of VGLUT1-containing SVs in neurons *in vitro* and *in vivo*. The new model reports the localization and trafficking of VGLUT1 and VGLUT1-containing SVs with very high fidelity. Imaging of VGLUT1^{Venus} mice showed that glutamatergic SVs are constantly trafficked and exchanged between synapses, indicating that presynaptic function and plasticity *in vivo* are regulated dynamically by the redistribution of a pansynaptic superpool of SVs.

Validity and assets of the VGLUT1^{Venus} KI mouse model

The generation of the VGLUT1^{Venus} KI mouse model involved tagging of an SV protein with a genetically encoded fluorescent protein of the GFP family. Instead of EYFP, which we had used previously in a Munc13-1^{EYFP} KI mouse line (Kalla et al., 2006), we selected Venus as the tag because of its faster folding and brighter fluorescence (Nagai et al., 2002). For selective tagging of

glutamatergic SVs, our options were restricted to VGLUT1. VGLUTs are the most specific markers of glutamatergic SVs, and among the known VGLUT isoforms, VGLUT1 is strongly expressed in brain regions that are readily amenable to *in vivo* imaging (Bellocchio et al., 1998; Takamori et al., 2000; Herzog et al., 2001; Varoqui et al., 2002). We opted for a KI mutagenesis strategy to achieve expression of VGLUT1^{Venus} at WT levels and according to the WT developmental expression profile. A possible disadvantage of this strategy is that VGLUT1^{Venus} expression covers the majority of forebrain glutamatergic synapses, which may be problematic for studies requiring the sparse mosaic labeling that is often obtained with transgenic models (Feng et al., 2000).

Our analyses of VGLUT1^{Venus} mice demonstrate that the new model meets all the expectations described above. In homozygous KIs, VGLUT1^{Venus} is expressed at the same level as WT VGLUT1 in WT mice. The developmental expression profile of VGLUT1^{Venus} and its regional, cellular, and subcellular distribution are indistinguishable from those of WT VGLUT1 (Figs. 1–3) (see also Bellocchio et al., 1998; Takamori et al., 2000; Herzog et al., 2001; Varoqui et al., 2002), VGLUT1^{Venus} retains the ability to interact specifically with EndophilinA1 and shows the same glutamate uptake efficacy as WT VGLUT1, and VGLUT1^{Venus} neurons show WT-like synaptic transmission and short-term plasticity characteristics (Fig. 4).

We conclude that VGLUT1^{Venus} mice are faithful live reporters of VGLUT1 and VGLUT1-positive SVs *in vitro* and *in vivo* and will be useful for many applications in neuroscience. For example, they can be used in combination with other manipulations (e.g., KOs, virus-mediated perturbations, disease models, or pharmacological or physiological alterations) for quantitative analyses of synaptogenesis, SV trafficking and turnover, or synapse elimination and degeneration. Given that the VGLUT complement and VGLUT expression levels at synapses affect quantal size and vesicular release probability (Wojcik et al., 2004; De Gois et al., 2005; Wilson et al., 2005; Herzog et al., 2006; Moechars et al., 2006; Weston et al., 2011), the dynamic changes of VGLUT1^{Venus} levels that can be observed in KI preparations (Figs. 5–8) represent an indirect live and *in vivo* readout of changes in presynaptic strength.

Intersynaptic exchange of VGLUT1-positive SVs

Our analyses of VGLUT1^{Venus} neuron cultures indicate that bouton-sized, stable fluorescent puncta display actively recycling SVs that are apposed to glutamatergic postsynapses (Fig. 3*A–D*) and can thus be assumed to represent presynapses. We therefore used our VGLUT1^{Venus} model for FRAP experiments *in vitro* and *in vivo*. Previously published FRAP analyses of SV mobility *in vitro* used heterologously expressed GFP-tagged SV-proteins or styryl dye labeling (Darcy et al., 2006; Tsuriel et al., 2006; Staras et al., 2010). Our VGLUT1^{Venus} model has distinct advantages over these methods, because overexpressed GFP-fusion proteins are prone to aberrant trafficking due to misexpression artifacts, and studies using styryl dye incorporation into endocytosed SVs cannot assess resting SVs and require multiple experimental manipulations of nerve cell activity in culture to stain SVs and to prevent dye release. Instead, our mouse model allows to image all VGLUT1 SVs (and other associated organelles) under unperturbed conditions (Figs. 5–8).

Our FRAP data show that under native conditions, 40% of VGLUT1^{Venus} in presynapses are exchanged within 1 h (0.7%/min). This is not due to a net loss of VGLUT1 caused by degradation or to *de novo* synthesis, which is negligible at a timescale of up to 5 h (Fig. 5*E*,*F*). Thus, most of the incremental changes in synaptic VGLUT1^{Venus} content result from gradual transfer between presynaptic sites of the same axon (Fig. 8*B*,*C*). Our findings corroborate recent studies showing that SVs are exchanged between presynaptic boutons along axons of cultured neurons. The styryl dye-labeled structures examined in these studies mostly reflected SV-like organelles of 40 nm diameter that retained release competence upon reincorporation into new synapses (Darcy et al., 2006; Staras et al., 2010). Therefore, and because VGLUT1 is hardly detectable in compartments other than SVs (Balaji and Ryan, 2007), we conclude that most mobile VGLUT1^{Venus} structures monitored here correspond to SVs.

Interestingly, 15% of synapses in cultured neurons showed large and sudden VGLUT1^{Venus} fluorescence changes, including elimination or generation of stable SV clusters (Fig. 7*C*), which likely reflect more profound rearrangements that may also involve active zones, postsynaptic densities, or VGLUT1 associated with transport cargo or endosomes. As signaling molecules such as BDNF can perturb the stability of SV clusters at synapses (Staras et al., 2010), some of the fluorescence changes we observed may reflect such regulatory processes.

Incomplete biphasic recovery of VGLUT1^{Venus} fluorescence occurred within 1 h upon FRAP (Figs. 5, 6). The faster FRAP component likely reflects SVs that transit through the bleached area via axonal transport, whereas the slow FRAP component may indicate the exchange of SVs between axonal transport tracks and SV clusters (Darcy et al., 2006; Tsuriel et al., 2006). The FRAP characteristics *in vivo* were qualitatively similar to those *in vitro*, but the overall recovery was 10% smaller. The pool of slowly replenishing VGLUT1 SVs was mainly affected (23% compared to 33% *in vitro*) and the recovery time constants τ_F and τ_S were longer (3.7 min and 44.5 min vs 44 s and 28.5 min *in vitro*), indicating that the mobile fraction of SVs is smaller *in vivo*. These differences likely reflect the different state of intact networks in the cerebral cortex of adult mice (support by glial cells, modulatory inputs from aminergic neurons, anesthetics, etc.) as compared to DIV18 hippocampal neuronal networks *in vitro* (less developed networks, effects of culture medium, etc.). The similar amplitude of the fast FRAP phase *in vitro* and *in vivo* may indicate that axonal transport is less sensitive to the state of a neuron than presynaptic composition and integrity, which is expected to affect the slow recovery. Based on these arguments, analyses of cultured neurons would represent a valid approach to analyze SV trafficking in the VGLUT1^{Venus} model. However, we cannot exclude that SV trafficking and mobility are inherently different *in vivo* and *in vitro*, stressing the importance of our VGLUT1^{Venus} KI for future *in vivo* studies.

Some 60% of the VGLUT1^{Venus} fluorescence at synapses remained stable over 1 h (Figs. 4*B*, 5*C*). A similar proportion of SVs was previously found to form a reluctantly releasable resting SV pool (Harata et al., 2001). It is possible that the stable SV pool that we and others (Staras et al., 2010) observed in imaging studies reports this reluctantly releasable resting SV pool. Relationships between these resting/stable pools will be of key interest to understand the pathways through which SVs reach fusion competence at active zones (Kim and Ryan, 2010).

Dynamics and homeostasis of VGLUT1-positive SV content in synapse populations

According to our time-lapse imaging experiments, 60% of all presynaptic boutons show persistent and balanced increases or decreases of their VGLUT1^{Venus} content of ~30% in the course of 1 h (i.e., 32% upregulation, 29% downregulation), so that the

total SV number in the terminals remained unchanged (Fig. 8). This is expected to cause alterations of synaptic strength at the affected presynaptic terminals, e.g., by changing the availability of release competent SVs (Staras et al., 2010), the synaptic release probability (Weston et al., 2011), or the VGLUT1 concentration per SV, resulting in quantal size changes (Wojcik et al., 2004; Wilson et al., 2005; Moechars et al., 2006; Balschun et al., 2010). The latter scenario may involve local membrane trafficking that we were unable to resolve (Hoopmann et al., 2010). Complementing a previous study, which identified a superpool of SVs that is shared by several presynaptic terminals along an axon (Staras et al., 2010), our data indicate that SVs are exchanged among large ensembles of presynapses in unperturbed neurons. Such SV redistribution in synapse networks may represent plastic processes of synapse strengthening or weakening that would not be detectable by most standard electrophysiological assays that assess synaptic inputs at the level of whole cells. Given that our new VGLUT1^{Venus} model allows for the simultaneous imaging of many single presynapses over time, its combination with electrophysiological or optogenetic approaches is likely to provide new insights into synapse homeostasis and plasticity that have so far not been achievable.

References

Augustin I, Rosenmund C, Südhof TC, Brose N (1999) Munc13–1 is essential for fusion competence of glutamatergic synaptic vesicles. Nature 400:457–461.

Balaji J, Ryan TA (2007) Single-vesicle imaging reveals that synaptic vesicle exocytosis and endocytosis are coupled by a single stochastic mode. Proc Natl Acad Sci U S A 104:20576–20581.

Balschun D, Moechars D, Callaerts-Vegh Z, Vermaercke B, Van Acker N, Andries L, D'Hooge R (2010) Vesicular glutamate transporter VGLUT1 has a role in hippocampal long-term potentiation and spatial reversal learning. Cereb Cortex 20:684–693.

Bellocchio EE, Hu H, Pohorille A, Chan J, Pickel VM, Edwards RH (1998) The localization of the brain-specific inorganic phosphate transporter suggests a specific presynaptic role in glutamatergic transmission. J Neurosci 18:8648–8659.

Boulland J-L, Qureshi T, Seal RP, Rafiki A, Gundersen V, Bergersen LH, Fremeau RT Jr, Edwards RH, Storm-Mathisen J, Chaudhry FA (2004) Expression of the vesicular glutamate transporters during development indicates the widespread corelease of multiple neurotransmitters. J Comp Neurol 480:264–280.

Brose N, Huntley GW, Stern-Bach Y, Sharma G, Morrison JH, Heinemann SF (1994) Differential assembly of coexpressed glutamate receptor subunits in neurons of rat cerebral cortex. J Biol Chem 269:16780–16784.

Chen X, Barg S, Almers W (2008) Release of the styryl dyes from single synaptic vesicles in hippocampal neurons. J Neurosci 28:1894–1903.

Darcy KJ, Staras K, Collinson LM, Goda Y (2006) Constitutive sharing of recycling synaptic vesicles between presynaptic boutons. Nat Neurosci 9:315–321.

De Gois S, Schäfer MK-H, Defamie N, Chen C, Ricci A, Weihe E, Varoqui H, Erickson JD (2005) Homeostatic scaling of vesicular glutamate and GABA transporter expression in rat neocortical circuits. J Neurosci 25:7121–7133.

Feng G, Mellor RH, Bernstein M, Keller-Peck C, Nguyen QT, Wallace M, Nerbonne JM, Lichtman JW, Sanes JR (2000) Imaging neuronal subsets in transgenic mice expressing multiple spectral variants of GFP. Neuron 28:41–51.

Fremeau RT Jr, Troyer MD, Pahner I, Nygaard GO, Tran CH, Reimer RJ, Bellocchio EE, Fortin D, Storm-Mathisen J, Edwards RH (2001) The expression of vesicular glutamate transporters defines two classes of excitatory synapse. Neuron 31:247–260.

Fremeau RT Jr, Voglmaier S, Seal RP, Edwards RH (2004a) VGLUTs define subsets of excitatory neurons and suggest novel roles for glutamate. Trends Neurosci 27:98–103.

Fremeau RT Jr, Kam K, Qureshi T, Johnson J, Copenhagen DR, Storm-Mathisen J, Chaudhry FA, Nicoll RA, Edwards RH (2004b) Vesicular glutamate transporters 1 and 2 target to functionally distinct synaptic release sites. Science 304:1815–1819.

Gähwiler BH (1981) Organotypic monolayer cultures of nervous tissue. J Neurosci Methods 4:329–342.

Galli T, Haucke V (2001) Cycling of synaptic vesicles: how far? How fast! Sci STKE 2001:re1.

Giepmans BN, Adams SR, Ellisman MH, Tsien RY (2006) The fluorescent toolbox for assessing protein location and function. Science 312:217–224.

Harata N, Ryan TA, Smith SJ, Buchanan J, Tsien RW (2001) Visualizing recycling synaptic vesicles in hippocampal neurons by FM 1–43 photoconversion. Proc Natl Acad Sci U S A 98:12748–12753.

Herzog E, Bellenchi GC, Gras C, Bernard V, Ravassard P, Bedet C, Gasnier B, Giros B, El Mestikawy S (2001) The existence of a second vesicular glutamate transporter specifies subpopulations of glutamatergic neurons. J Neurosci 21:RC181.

Herzog E, Takamori S, Jahn R, Brose N, Wojcik SM (2006) Synaptic and vesicular co-localization of the glutamate transporters VGLUT1 and VGLUT2 in the mouse hippocampus. J Neurochem 99:1011–1018.

Hisano S, Sawada K, Kawano M, Kanemoto M, Xiong G, Mogi K, Sakata-Haga H, Takeda J, Fukui Y, Nogami H (2002) Expression of inorganic phosphate/vesicular glutamate transporters (BNPI/VGLUT1 and DNPI/VGLUT2) in the cerebellum and precerebellar nuclei of the rat. Brain Res Mol Brain Res 107:23–31.

Hoopmann P, Punge A, Barysch SV, Westphal V, Bückers J, Opazo F, Bethani I, Lauterbach MA, Hell SW, Rizzoli SO (2010) Endosomal sorting of readily releasable synaptic vesicles. Proc Natl Acad Sci U S A 107:19055–19060.

Huttner WB, Schiebler W, Greengard P, De Camilli P (1983) Synapsin I (protein I), a nerve terminal-specific phosphoprotein. III. Its association with synaptic vesicles studied in a highly purified synaptic vesicle preparation. J Cell Biol 96:1374–1388.

Jin Y, Garner CC (2008) Molecular mechanisms of presynaptic differentiation. Annu Rev Cell Dev Biol 24:237–262.

Jones DH, Matus AI (1974) Isolation of synaptic plasma membrane from brain by combined flotation-sedimentation density gradient centrifugation. Biochim Biophys Acta 356:276–287.

Kalla S, Stern M, Basu J, Varoqueaux F, Reim K, Rosenmund C, Ziv NE, Brose N (2006) Molecular dynamics of a presynaptic active zone protein studied in Munc13-1-enhanced yellow fluorescent protein knock-in mutant mice. J Neurosci 26:13054–13066.

Kaneko T, Fujiyama F, Hioki H (2002) Immunohistochemical localization of candidates for vesicular glutamate transporters in the rat brain. J Comp Neurol 444:39–62.

Khvotchev M, Kavalali ET (2008) Pharmacology of neurotransmitter release: measuring exocytosis. Handb Exp Pharmacol 23–43.

Kim SH, Ryan TA (2010) CDK5 serves as a major control point in neurotransmitter release. Neuron 67:797–809.

Lakso M, Pichel JG, Gorman JR, Sauer B, Okamoto Y, Lee E, Alt FW, Westphal H (1996) Efficient in vivo manipulation of mouse genomic sequences at the zygote stage. Proc Natl Acad Sci U S A 93:5860–5865.

McAnaney TB, Zeng W, Doe CFE, Bhanji N, Wakelin S, Pearson DS, Abbyad P, Shi X, Boxer SG, Bagshaw CR (2005) Protonation, photobleaching, and photoactivation of yellow fluorescent protein (YFP 10C): a unifying mechanism. Biochemistry 44:5510–5524.

Mimura Y, Mogi K, Kawano M, Fukui Y, Takeda J, Nogami H, Hisano S (2002) Differential expression of two distinct vesicular glutamate transporters in the rat retina. Neuroreport 13:1925–1928.

Moechars D, Weston MC, Leo S, Callaerts-Vegh Z, Goris I, Daneels G, Buist A, Cik M, van der Spek P, Kass S, Meert T, D'Hooge R, Rosenmund C, Hampson RM (2006) Vesicular glutamate transporter VGLUT2 expression levels control quantal size and neuropathic pain. J Neurosci 26:12055–12066.

Nagai T, Ibata K, Park ES, Kubota M, Mikoshiba K, Miyawaki A (2002) A variant of yellow fluorescent protein with fast and efficient maturation for cell-biological applications. Nat Biotechnol 20:87–90.

Pologruto TA, Sabatini BL, Svoboda K (2003) ScanImage: flexible software for operating laser scanning microscopes. Biomed Eng Online 2:13.

Pyott SJ, Rosenmund C (2002) The effects of temperature on vesicular supply and release in autaptic cultures of rat and mouse hippocampal neurons. J Physiol 539:523–535.

Rhee JS, Betz A, Pyott S, Reim K, Varoqueaux F, Augustin I, Hesse D, Südhof TC, Takahashi M, Rosenmund C, Brose N (2002) Beta phorbol ester-

and diacylglycerol-induced augmentation of transmitter release is mediated by Munc13s and not by PKCs. Cell 108:121–133.
Rizzoli SO, Betz WJ (2005) Synaptic vesicle pools. Nat Rev Neurosci 6:57–69.
Rizzoli SO, Richards DA, Betz WJ (2003) Monitoring synaptic vesicle recycling in frog motor nerve terminals with FM dyes. J Neurocytol 32:539–549.
Rosenmund C, Stevens CF (1996) Definition of the readily releasable pool of vesicles at hippocampal synapses. Neuron 16:1197–1207.
Sakata-Haga H, Kanemoto M, Maruyama D, Hoshi K, Mogi K, Narita M, Okado N, Ikeda Y, Nogami H, Fukui Y, Kojima I, Takeda J, Hisano S (2001) Differential localization and colocalization of two neuron-types of sodium-dependent inorganic phosphate cotransporters in rat forebrain. Brain Res 902:143–155.
Staras K, Branco T, Burden JJ, Pozo K, Darcy K, Marra V, Ratnayaka A, Goda Y (2010) A vesicle superpool spans multiple presynaptic terminals in hippocampal neurons. Neuron 66:37–44.
Takamori S, Rhee JS, Rosenmund C, Jahn R (2000) Identification of a vesicular glutamate transporter that defines a glutamatergic phenotype in neurons. Nature 407:189–194.
Thomas KR, Capecchi MR (1987) Site-directed mutagenesis by gene targeting in mouse embryo-derived stem cells. Cell 51:503–512.
Tsuriel S, Geva R, Zamorano P, Dresbach T, Boeckers T, Gundelfinger ED, Garner CC, Ziv NE (2006) Local sharing as a predominant determinant of synaptic matrix molecular dynamics. PLoS Biol 4:e271.
Varoqui H, Schäfer MKH, Zhu H, Weihe E, Erickson JD (2002) Identification of the differentiation-associated Na+/PI transporter as a novel vesicular glutamate transporter expressed in a distinct set of glutamatergic synapses. J Neurosci 22:142–155.
Vinatier J, Herzog E, Plamont M-A, Wojcik SM, Schmidt A, Brose N, Daviet L, El Mestikawy S, Giros B (2006) Interaction between the vesicular glutamate transporter type 1 and endophilin A1, a protein essential for endocytosis. J Neurochem 97:1111–1125.
Voglmaier SM, Kam K, Yang H, Fortin DL, Hua Z, Nicoll RA, Edwards RH (2006) Distinct endocytic pathways control the rate and extent of synaptic vesicle protein recycling. Neuron 51:71–84.
Weston MC, Nehring RB, Wojcik SM, Rosenmund C (2011) Interplay between VGLUT isoforms and endophilin A1 regulates neurotransmitter release and short-term plasticity. Neuron 69:1147–1159.
Wilson NR, Kang J, Hueske EV, Leung T, Varoqui H, Murnick JG, Erickson JD, Liu G (2005) Presynaptic regulation of quantal size by the vesicular glutamate transporter VGLUT1. J Neurosci 25:6221–6234.
Wojcik SM, Brose N (2007) Regulation of membrane fusion in synaptic excitation-secretion coupling: speed and accuracy matter. Neuron 55:11–24.
Wojcik SM, Rhee JS, Herzog E, Sigler A, Jahn R, Takamori S, Brose N, Rosenmund C (2004) An essential role for vesicular glutamate transporter 1 (VGLUT1) in postnatal development and control of quantal size. Proc Natl Acad Sci U S A 101:7158–7163.